Power Management of a Grid Forming Enabled Hybrid Energy System

by

Echezona Ugonna Ezeodili.

A thesis submitted to the Graduate Faculty of
Auburn University
in partial fulfillment of the requirements for the Degree of
Master of Science (MSc)

Auburn Alabama
December 11, 2021.

Keywords: renewable energy, wind energy, hybrid system, hydrogen, battery storage, PSCAD

Approved by:
Eduard Muljadi, Chair, Professor of Electrical and Computer Engineering
R. Mark Nelms, Department Chair Professor of Electrical and Computer Engineering
Mark Halpin, Alabama Power Company Professor of Electrical and Computer Engineering

Abstract:

Hybrid power generation systems that combine different renewable energy sources and energy storage systems offer an environmentally friendly alternative to conventional power generators for stand-alone applications. However, the displacement of synchronous generators with inverter-based resources reduces the overall inertia and, hence, the power system's resilience. Also, the intermittency of these renewable resources necessitates the need for additional storage devices to balance the power generated and power demand.

This thesis investigates the effectiveness of an active power management strategy in maintaining the stability of a stand-alone power system comprising of a Wind Turbine Generator (WTG), Fuel Cell (FC), Electrolyzer (EZ) and Battery Energy Storage System (BESS). In an islanding mode, the inverter-interfaced resource operates in Grid Forming mode (GFM) while ensuring a power balance between the generation and demand.

The proposed scheme was modeled and simulated under different case studies to verify the management strategy using PSCAD/EMTDC.

Acknowledgement:

I would like to thank my advisor, Professor Eduard Muljadi, who gave me the latitude to explore my research interests and provide guidance whenever needed. I also appreciate Dr. Jinho Kim, who was helpful and available to share his knowledge and helped answer any questions I had regarding my research. I would also like to thank my fellow research mates in the Auburn University power group for their encouragement and solidarity in our academic pursuits.

I also want to thank my family and friends who continually provided financial, emotional, and spiritual support to me in this journey. I am grateful that they get to see the outcome of their labor.

Lastly, I would like to thank God, without whom this would be impossible.

Table of Content:

List of Figures:

List of Tables:

Chapter 1: Introduction

1.1 Background and Motivation:

Electricity has become a dominant variable of any economy; it is crucial for poverty alleviation, economic growth, and improved living standards. Electricity also plays a pivotal role in the fields of transportation, medicine, and entertainment. However, according to a recent global study [1], over 940 million people globally do not have access to electricity, with about two-thirds of that population in sub-Saharan Africa. This number rises as many developing countries struggle to cushion the effect of the pandemic [2], and direct resources to immediate economic relief projects, further pushing many countries farther away from achieving the goal of universal access to electricity by 2030.

In recent years, the world has turned to renewable energy for a cleaner and economical energy focused society. This resource answers the growing concerns of climate change across the globe caused by most conventional electricity generation methods. As the world population is continually rising and energy demand increases accordingly, Renewable Energy Sources (RES) pose a great solution in achieving these goals. The abundance of solar, wind, hydro, and biomass ensure a continuous supply of clean energy for generating electricity. Moreover, the advancement of renewable energy research made possible by technological breakthroughs has made renewable technologies cheaper and far more ubiquitous than they were in previous years.

Nowadays, distributed power systems are gaining great attention due to the advantages of being more reliable, easily scalable, and flexibly controlled than large centralized power systems. The microgrid is emerging as a potential concept to realize this distributed power system paradigm. The integration of renewable energy sources (RES), energy storage systems (ESS), and dynamic loads makes it possible for microgrids to operate in grid-connected mode and exchange power with the main utility, or in islanded/stand-alone mode to supply local loads when the grid is not present. Microgrids and

Distributed Energy Resources have become an exciting field of research to cater to people without grid connection, or where grid connection is not technically or economically viable.

1.1.1 Future Trend of Renewable Power Generation:

This century expects to witness unprecedented growth and challenges in power generation, delivery, and usage. Environmentally friendly (renewable and clean alternatives) power generation technologies play an essential role in future power supply due to increased global public awareness of the need for environmental protection and desire for less dependence on fossil fuels for energy production. These technologies include power generation from renewable energy (RE) resources, such as wind, photovoltaic (PV), micro-hydro (MH), biomass, geothermal, ocean wave and tides, and clean alternative energy (AE) power generation technologies such as fuel cells (FCs) and microturbines (MTs). Figure 1 below shows the distribution of fuel shares in the world's total primary energy supply and product shares in the world's renewable energy supply according to data by the United States Energy Information Administration (EIA) from 2020.

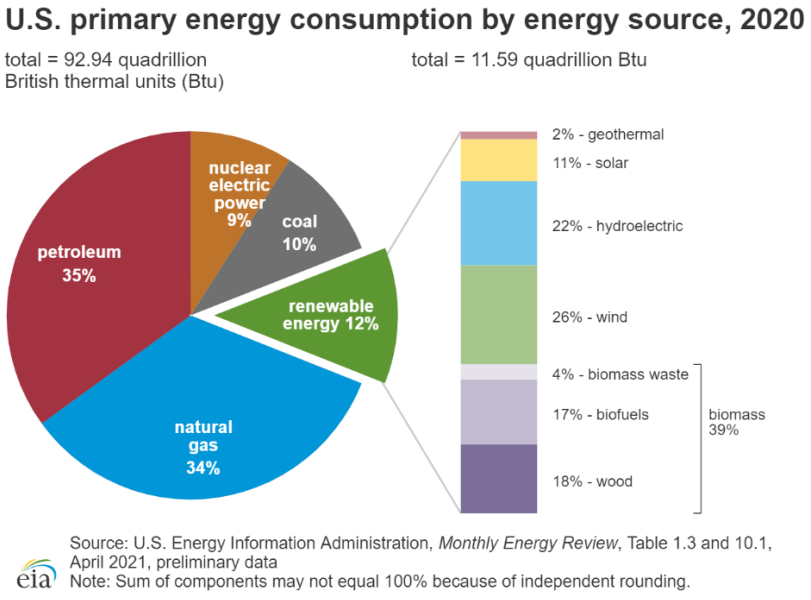

Fig 1: 2020 shares in world total energy supply

Source: INTERNATIONAL ENERGY AGENCY (IEA)

Also, according to the US EIA projection, as shown in figure 2 below, non-hydro renewable power generation continues its growth well into the future.

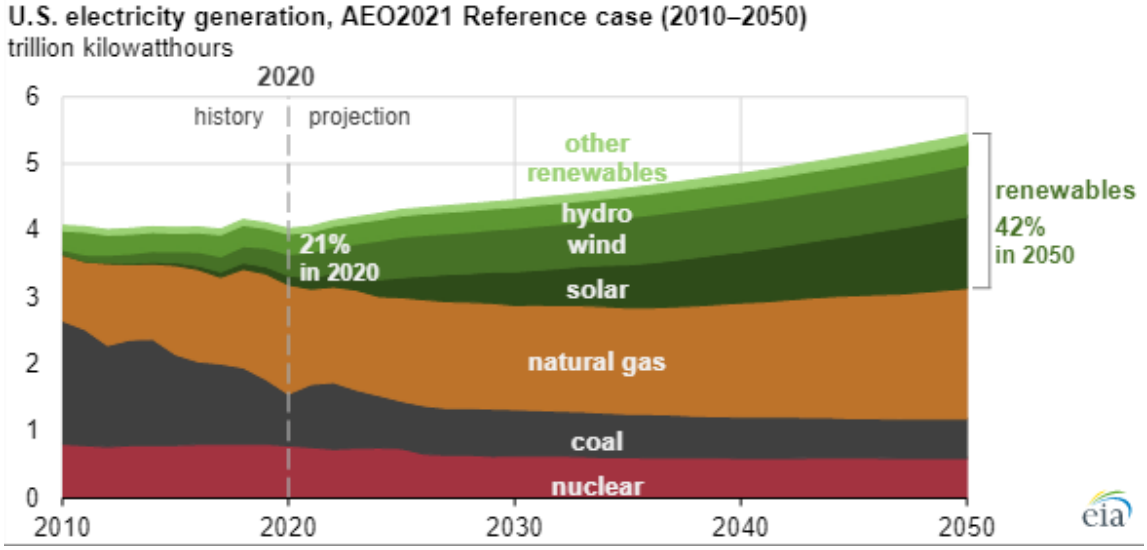

Figure 2: Renewable energy penetration forecast

Source: INTERNATIONAL ENERGY AGENCY (IEA)

One of the most promising applications of renewable energy technology is the installation of hybrid energy systems, especially in remote areas, where both grid extension and fuel costs are expensive. Different energy sources and converters are integrated for extended energy usage to meet sustained load demands under varying natural conditions. The Hybrid Energy System (HES) describes an energy system that combines renewable and conventional energy sources with energy storage technologies, power conditioning equipment, and a controller [3]. Hence, hybrid energy systems are gaining ground to drive renewable energy proliferation in developing the future electricity grid. In general, hybrid energy systems consist of combining several energy sources and storage units within the same system to optimize production and energy management.

1.1.2 Wind Energy Conversion System:

Over the past few years, wind power, in particular, has proliferated and is gradually becoming a

ubiquitous form of renewable energy. According to the American Wind Energy Association, the US wind power capacity increased by 8 percent in 2019, more than double the capacity the US had in 2010 [4].

The Wind Energy Conversion System (WECS) converts the kinetic energy of the wind speed into electrical energy. Typically, a WECS consists of wind turbine blades, an electric generator, power conditioning, and a control system. Different configurations of WECS are available based on the power-regulation mechanism employed (stall-regulated or pitch-regulated) and the type of generator used (synchronous or asynchronous). The wind turbines are also classified into vertical axis or horizontal axis turbines based on the structure of the turbine blades [5].

There are mainly four types of wind turbine generator technologies commonly installed.

a) **Constant Speed Squirrel-Cage Induction Generator.**
b) **Variable Slip Wind Turbine Generator**
c) **Variable Speed Wind Turbine Generator with Doubly Fed Induction Generator.**
d) **Variable speed wind turbine generator with full converter.**

This thesis employs the use of a type 4 WTG. In a type 4 wind turbine generator, an AC generator can be used as a variable speed generator. If a high-speed AC generator is used, a gear box is still needed. For a low-speed AC generator, a direct drive generator can be used without a gearbox. The power converter (at full rating) has two different sides, the Machine Side Converter (MSC operated at variable frequency) connected to the generator and the Line Side Converter (LSC operated at 60Hz) connected to the grid or directly to the load in a stand-alone connection. The synchronous generator is commonly used (i.e., Permanent Magnet or Wound Field). The speed can vary from 100% down to 10% below synchronous speed. Under short circuit conditions, the power converter limits its output current to its upper limit.

1.2 Challenges of renewable energy penetration:

Although renewable energy systems continue to show great promise, there are some issues associated with integrating renewable energy resources to the existing power network. The integration of the renewable energy sources (such as wind, solar, etc.) to the utility grids reduces the inertia due to the replacement of conventional synchronous generators. Thus, the frequency response of the power network is affected, which may lead to several issues such as under-frequency, load-shedding, and generator damage reducing the overall system reliability [6].

Furthermore, the intermittency of renewable resources causes active and reactive power imbalance in the system which generally affects the quality of power delivered by the network. Voltage variations, flickers, harmonic generation and load unbalance are the major power quality problems that may occur due to the fluctuations of renewable energy supply and the power electronics interface between the renewable energy generating system and the load. These power quality problems are not desirable and should be mitigated [7].

1.2.1 Energy storage technologies as a solution:

Energy storage systems (ESS) are an integral part of power systems with integrated renewable energy resources. Due to the intermittency and variability of Renewable Energy Sources (RES), energy storage technologies have been utilized to compensate power generated for continuous and reliable operation, especially in stand-alone power systems. Demand for new energy storage systems is increasing for applications such as remote area power supply systems (like offshore platforms, telecommunication installations), stressed electricity supply systems, emergency backup, and mobile applications.

ESS can help maintain the balance between demand and supply in an energy system, assisting in system reliability by providing backup power during electricity shortages or consuming

power during electricity surpluses. ESS find applications in various cases. In [8], a grid-scale battery energy storage is investigated for frequency support at grid level transmission. The battery provides an inertial response and improves the system frequency response. Also, in [9], an energy storage device is employed to assist a double-fed induction generator in providing the required reactive power to the grid during grid faults, providing voltage support. Other energy storage applications in microgrids include low voltage ride-through (LVRT), oscillation damping, and fluctuation suppression as well as in long term applications like load levelling, peak shaving, etc.

1.2.2 Hydrogen Energy Storage: Prospects.

Hydrogen technology combining fuel cells and electrolyzers with storage tanks is gaining momentum as a potential future energy storage medium to supplement various renewable energy sources. It has become a major power source for fuel cell-powered vehicles and for energy storage applications in power systems. The energy, stored as hydrogen in the form of a gas or a liquid, will never dissipate until it is used, making it a good application for emergency generators and other mission-critical energy applications.

Hydrogen storage proves advantageous for long-term energy storage as it provides unlimited energy capacity compared to battery energy storage or supercapacitors which lose the energy stored in them over time and need to be periodically recharged.

Hydrogen storage technologies are well suited for large scale applications compared to other storage methods. Unlike pumped hydro and compressed air storage, they are not restricted by geographical requirements [10]. More so, multiple hydrogen storage tanks can be deployed and produced hydrogen can be utilized on-site or transported to a place of need to fuel hydrogen cars or other applications.

Existing commercial hydrogen production methods include water electrolysis, multi-fuel gasification, and natural gas reforming. Natural gas reforming involves producing hydrogen from natural gas which contains methane that can be used to produce hydrogen with thermal processes, such as steam-methane reformation and partial oxidation. Most hydrogen produced today in the US is made via steam-methane reforming [11]. On the other hand, the water electrolyzer is a promising and cleaner method of hydrogen production, especially when energized by renewable energy sources (photovoltaics, wind power, etc.). This process involves utilizing renewables to power electrolysis, a process in which an electrical current is passed through a chemical solution in order to separate hydrogen. Once hydrogen is created through electrolysis it is stored and can be used in stationary fuel cells to supply energy during high energy demand periods or utilized as fuels in hydrogen-powered vehicles.

1.3 Problem statement:

Although converter-based renewable resources can secure the electrical energy for future power systems while the energy storage technologies are capable in backing up the intermittency of the renewables, they however reduce the overall system inertia compared to a conventional power system causing nominal deviations.

Therefore, as power electronic-based systems continue to replace conventional power plants, the systems should be equipped with effective control methods, particularly inverter controls that can provide enough system inertia to maintain the overall system's resilience and power [12].

Grid Forming Inverters can operate as virtual synchronous generators providing voltage and frequency references ensuring the voltage and frequency stability of the power system under normal and emergency conditions [13]. This implies that effective power management and converter control

methods are necessary for hybrid power systems to maintain the system's effective operation stability. This is important especially if the system is supplying sensitive load such as hospitals, military equipment, etc.

Therefore, this thesis proposes power management of a grid-forming enabled hybrid power system consisting of a type-4 wind turbine with fuel cell, electrolyzer, and battery energy storage. The energy storage systems maintain the balance between demand and supply by regulating the DC link voltage according to their storage limits. Under any wind speed or load demand change, the battery storage system provides or consumes the transient power due to its faster dynamics than its fuel cell/electrolyzer counterparts, which serve as backup power. The proposed scheme was tested considering wind and load variations using PSCAD software.

1.4 Research objectives:

This thesis aims to develop a system that achieves the following:

- To achieve effective power management control coordination among the wind generator and energy storage system (battery fuel cell and electrolyzer) to maintain power balance by keeping the DC-link voltage of the wind turbine generator constant.
- To extract maximum power from wind turbine generators under variable wind speed conditions.
- To develop a GFM inverter with virtual synchronous generator capabilities to ensure voltage and frequency stability of the system.
- To examine the concepts through a developed hybrid energy system in PSCAD/EMTDC.

1.5 Research methodology:

This thesis investigates the local controls in a test system containing a type 4 WTG, PEM Fuel Cell (FC), Battery Energy Storage System (BESS), and a hydrogen electrolyzer (ELZ) to manage and maintain the power between generation and demand. The simulation employs the average model of the WTG and converter systems for faster yet accurate simulation results. Therefore, neither harmonic oscillation nor losses related to the converters are considered. The system is assumed to be balanced, and it is focused on steady-state behavior.

The test system is modeled in PSCAD/EMTDC and simulated under different scenarios to study the effectiveness of the power management control method developed,

1.6 Thesis outline:

The thesis outline is as follows:

- Chapter one introduces the background and motivation for the project and the objectives and methodology of the thesis.
- Chapter two discusses the system description and explains the theoretical operation of each component in the system.
- Chapter three discusses the power management control methodology employed in the test system.
- Chapter four discusses the simulation and results.
- Chapter five is for the conclusion and future work.

Chapter 2: Theoretical Modelling and Analysis of the System Components

2.1 System description:

This thesis presents a dynamic model of a hybrid energy storage system consisting of a wind to hydrogen set incorporating a type-4 wind turbine generator (WTG), an alkaline electrolyzer (ELZ), PEM fuel cell (FC), hydrogen storage tank, and a Battery Energy Storage System (BESS). The system controllers operate based on parameters of the system components in order to keep the dc link voltage at the dc circuit of the wind turbine generator within its reference value.

Fig. 3 below shows the model of the system used in this thesis:

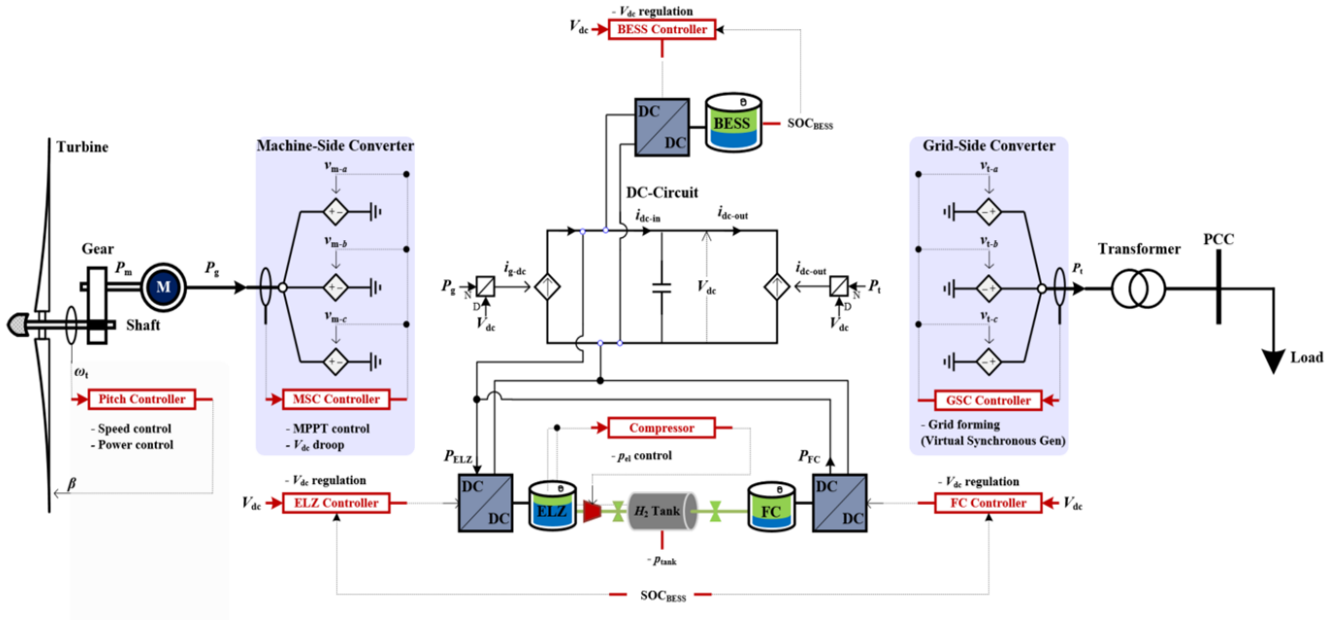

Figure 3: overview of hybrid power system

2.2 WECS modelling:

In order to determine the aerodynamic rotor power in wind (P_w), it is first necessary to calculate the amount of power in the wind. The kinetic energy E (in Joules) of an air mass M(kg) moving at a speed v_w can be expressed as [5]:

$$E = \frac{1}{2}.M.{V_w}^2 \quad (1)$$

If air density is ρ in kg/m^3, mass flow through an area A is given by:

$$\dot{M} = \rho.A.V_w \quad (2)$$

Therefore, an equation for the energy per second or power (Watts) through a cross-sectional area A normal to the wind can be derived as:

$$P_w = \frac{1}{2}.\rho.A.{V_w}^3 \quad (3)$$

In the case of wind turbines, area A is the area swept by the rotor blades, and since only a part of this power may be captured due to the non-ideal nature of the rotor, the rotor power coefficient c_p also needs to be included. Thus, the resulting power extracted by the wind turbine is given as:

$$P_w = \frac{1}{2}.\rho.\pi.R^2.{V_w}^3.c_p(\lambda,\beta) \quad (4)$$

where:

R_w is the blade radius of the wind turbine;

β is the blade pitch angle in degree;

λ is the tip speed ratio defined by:

$$\lambda = \frac{w_t.R}{V_w} \quad (5)$$

where:

w_t is the mechanical rotational speed of the turbine in rad/s

The aerodynamic efficiency of the wind turbine is maximum at $\beta = 0$ with an approximate value $c_{p,max} = 0.5$ for most applications.

In this thesis, c_p is expressed as a non-linear function of the tip speed ratio and the pitch angle as [5]:

$$c_p = 0.645\left\{0.00912\lambda + \frac{-5 - 0.4(2.5+\beta) + 116\lambda_i}{e^{21\lambda_i}}\right\} \quad (6)$$

where:

$$\lambda_i = \frac{1}{\lambda + 0.08(2.5+\beta)} - \frac{0.035}{1 + (2.5+\beta)^3} \quad (7)$$

The maximum output power of the wind turbine is obtained by tracking the rotor speed to the optimum point λ_{opt} that yields the maximum aerodynamic efficiency. From equation (5) the optimum wind turbine speed is given as:

$$w_{t,opt} = \frac{\lambda_{opt}.V_w}{R} \quad (8)$$

Therefore, the maximum power is obtained as:

$$P_{MPPT} = \frac{1}{2}.\rho.\pi.R^2.\left(\frac{w_{t,opt}.R}{\lambda_{opt}}\right)^3.c_{p,max} \quad (9)$$

which can be rewritten as:

$$P_{MPPT} = K_g {w_g}^3 \quad (10)$$

where K_g is the coefficient of the MPPT curve, defined as:

$$K_g = \frac{1}{2}.\rho.\pi.R^2.\left(\frac{R}{\lambda_{opt}}\right)^3.c_{p,max} \quad (11)$$

The figure 4 shows the plot of C_p vs TSR for different pitch angles [14]:

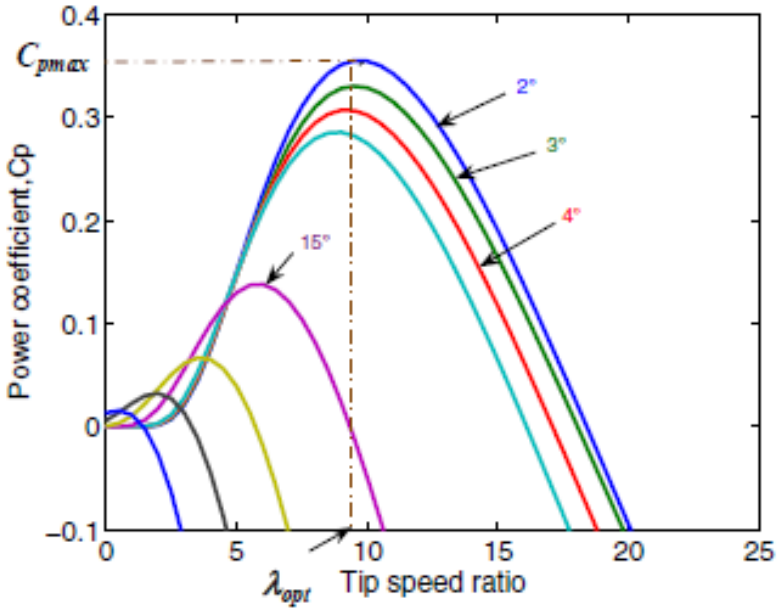

Figure 4: plot of Cp vs TSR

Figure 5 below shows the operation of the wind turbine under different wind conditions. It is seen that the wind turbine does not operate until a cut-in wind speed, $V_{cut\text{-}in}$ is achieved at which the wind turbine begins to generate power proportional to the wind speed. The WTG generates maximum power P_{rated} at the rated wind speed, and would operate at the optimal power with pitch-control, until a cut-off wind speed $V_{cut\text{-}off}$ is achieved at which the wind turbine does not generate any further power.

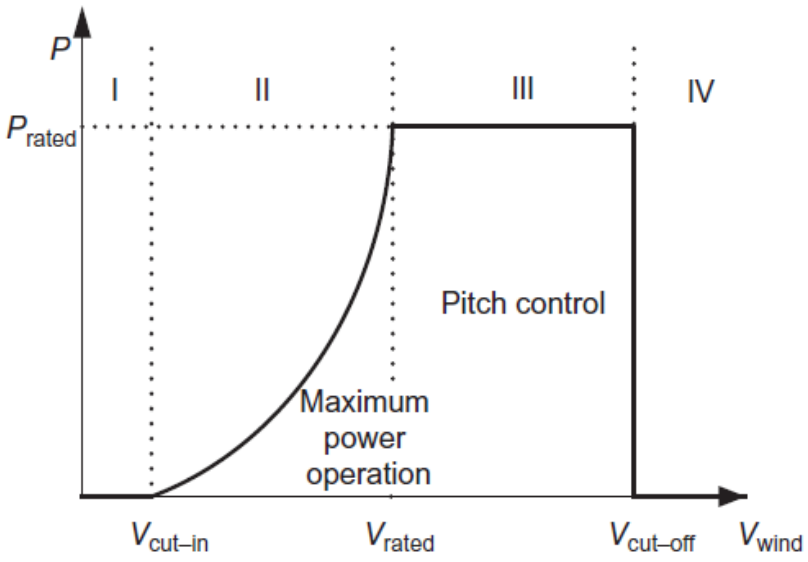

Figure 5: wind turbine power curve

2.2.1 Pitch angle control:

The WT model is coupled with dynamic pitch control to regulate the output power according to the curve in fig 5 so that it is capable of maintaining optimal power operation when the wind speed is above rated speed of the wind turbine.

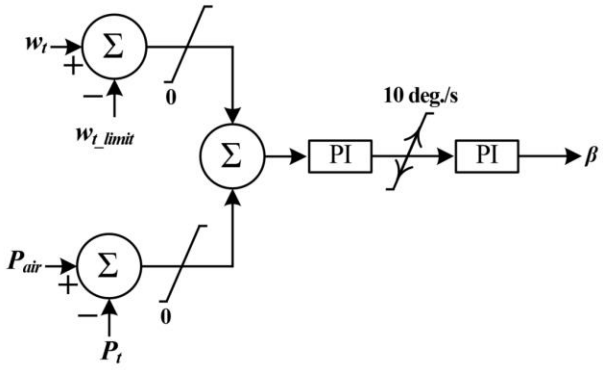

Figure 6: pitch controller of wind turbine

2.2.2 Drive Train Modelling:

Due to variation in wind speed, there will be aerodynamic torque fluctuations. These fluctuations interact with the dynamics of the drive train and modifies the torque transmitted. This modified torque can be assessed by the dynamic analysis of drive train model. Comparative study of wind

turbine generator drive train models show that the two-mass model is best suited for transient stability. The two-mass drive train model is shown below [15]:

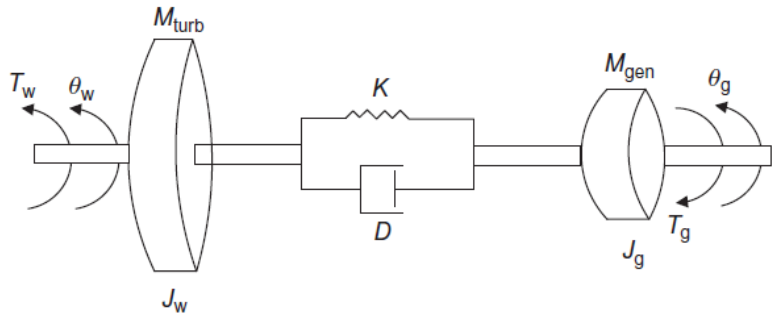

Figure 7: Two-mass drive train model

The differential equations governing the mechanical dynamics of the drive train are presented as follows [5]:

$$2H_t \frac{dw_t}{dt} = T_w - T_{sh} \tag{12}$$

$$2H_g \frac{dw_g}{dt} = T_{sh} - T_g \tag{13}$$

where:

H_t is the inertia constant of the turbine;

H_g is the inertia constant of the generator;

w_t is the angular speed of the wind turbine in p.u;

w_g is the angular speed of the generator in p.u;

T_{sh} is the shaft torque which is expressed:

$$T_{sh} = K_{sh}(\theta_t - \theta_g) + D_t\left(\frac{d\theta_t}{dt} - \frac{d\theta_g}{dt}\right) \quad (14)$$

θ_t is the angular position of turbine;

θ_t is the angular position of generator;

K_{sh} is the shaft stiffness;

D_t is the damping constant.

2.2.3. PMSG Modelling:

The PMSG is an essential component of the WTG. It consists of 3-phase stator winding while the rotor winding is replaced by permanent magnets. The elimination of the rotor field winding is beneficial for reducing copper losses, providing higher power density and lower rotor inertial and a more robust rotor construction. However, the disadvantages include loss of flexibility in field flux control and saturation of magnetic material over time [5].

The dynamic model of the permanent PMSG is derived from the two-phase synchronous reference frame in which the q-axis is 90° ahead of the d-axis with respect to the direction of rotation [16]. This is achieved by Park's Transformation. The mathematical expressions for this transformation from abc to dq reference frame are described in Appendix B.

The electrical model of the PMSG is given by the equations:

$$v_d = i_d R_s + L_d \frac{d}{dt}(i_d) - wL_q i_q \quad (15)$$

$$v_q = i_q R_s + L_q \frac{d}{dt}(i_q) - wL_d i_d + w\varphi_f \quad (16)$$

where:

v_d is the d-axis component of the stator voltage;

v_q is the q-axis component of the stator voltage;

R_s is the stator resistance;

i_d is the d-axis component of the stator current;

i_q is the q-axis component of the stator current;

w is the frequency;

φ_f is the flux linkage;

L_d is d-axis inductance of the generator;

L_q is q-axis inductance of the generator.

In this thesis, it is assumed that $L_d = L_q = L$. The q-axis counter electric potential $e_q = w\varphi_f$ and the d-axis counter electric potential $e_d = 0$.

Fig 8 shows the equivalent circuit of the PMSG on the dq-rotating reference frame.

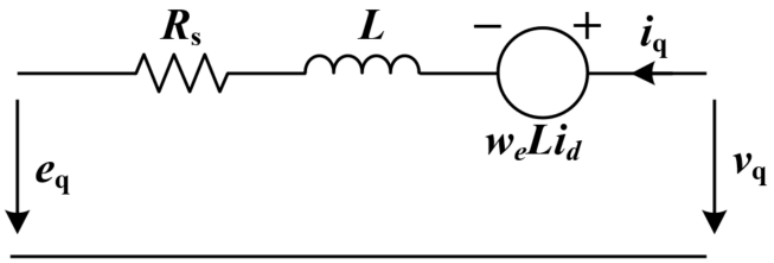

Figure 8a: d-axis equivalent circuit

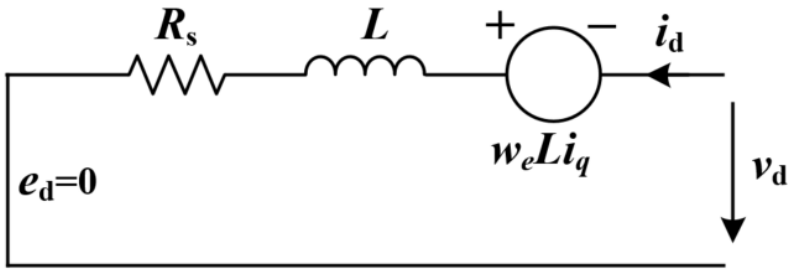

Figure 8b: q axis equivalent circuit.

The electromagnetic torque of the PMSG can be derived from:

$$T_e = 1.5 n_p \left((L_d - L_q) i_d i_q + i_q \varphi_f \right) \tag{17}$$

where:

n_p is the number of pole pairs.

As the inductances L_d and L_q are the equal, the above equation can be rewritten as:

$$T_e = 1.5 n_p i_q \varphi_f \tag{18}$$

2.3. Power Converter System:

A coordinated control strategy of back-to-back double pulse width modulation (PWM) converters is used to decouple the PMSG and the Wind Turbine from the rest of the power system. The power converter system consists of:

- A Machine Side Converter (MSC) which converts the AC power output of the PMSG into a variable DC voltage by a three-phase diode rectifier.
- A Grid Side Converter (GSC) which converts the DC voltage at the DC bus into the three-phase AC voltage at constant frequency.

2.3.1 Machine side converter (MSC) control:

The MSC aims to enable the WTG to operate in the MPPT operation. The rotor magnetic flux-oriented control technique is used for a decoupling control of d and q-axis stator current components of the PMSG [14]. The converter controls the generator rotor speed to achieve the maximum power operating point as long as V_{dc} is regulated at an acceptable range. The maximum power operating point acts as reference power signal for the MSC converter which is used to regulate the power generated by the PMSG of the wind turbine to produce reference signals ($I_{d\text{-}ref}$) that feed into the control loops.

Therefore, the machine side controller employs a cascaded control structure – a faster inner loop d-axis current control and a slower outer loop rotor power regulation control. The controller employs Pulse Width Modulation (PWM) technique to control the switching of the IGBT modules of the inverter. The MSC controller block is shown in fig 9 below:

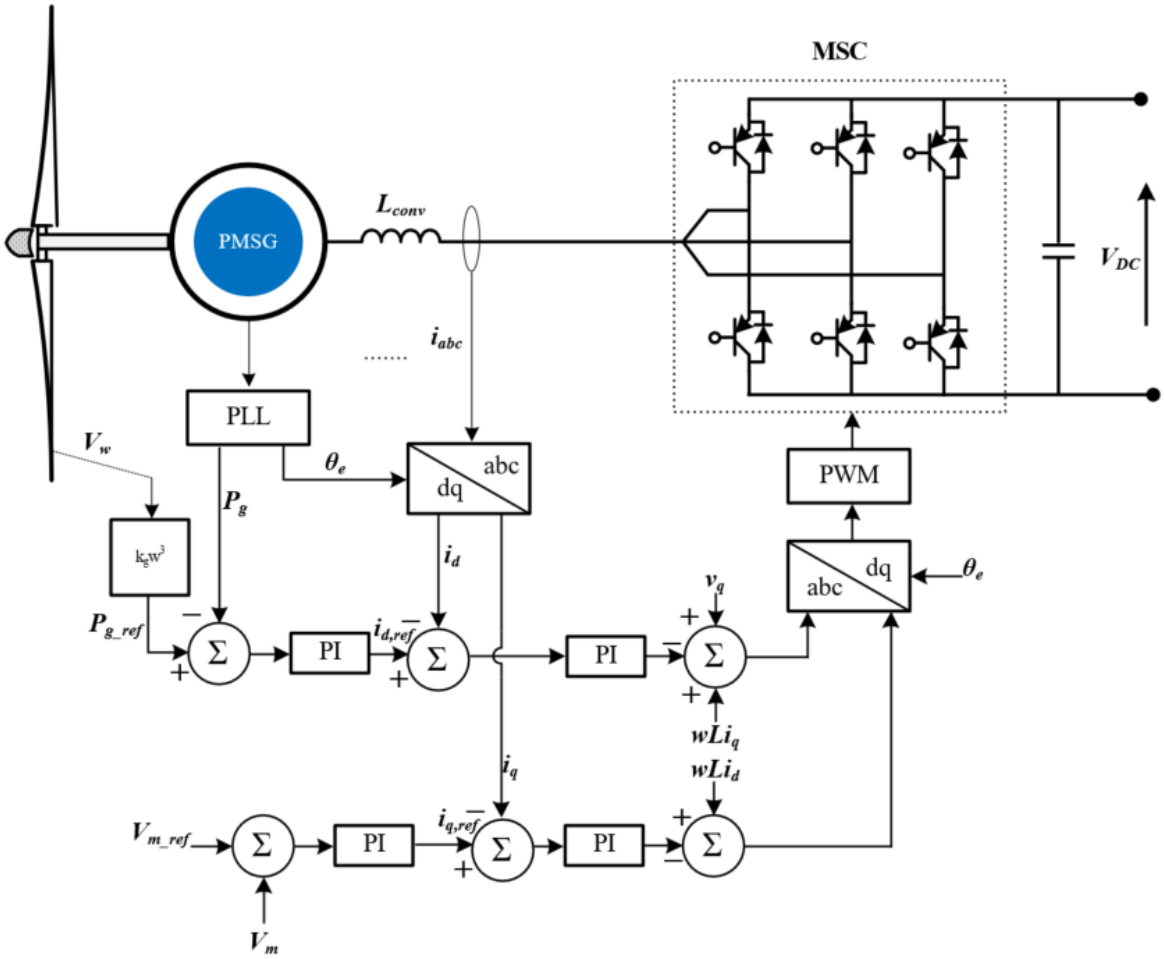

Figure 9: MSC controller of wind turbine

2.3.2 Grid Side Converter (GSC) control:

To provide Grid Forming (GFM) capability, the Grid Side Converter is designed to regulate the voltage and frequency at the point of common coupling. As there is no grid existing in a stand-alone system, the output voltages must be controlled in terms of amplitude and frequency [17].

To generate the desired frequency, the GSC controller virtually employs the concept of the swing equation that governs the conventional synchronous generator, which is expressed as follows:

$$w_{GSC} = \frac{1}{2H}\int \frac{P_{t-ref} - P_t}{w_{GSC}} \tag{19}$$

which generates the desired controller reference parameters as described by the block below:

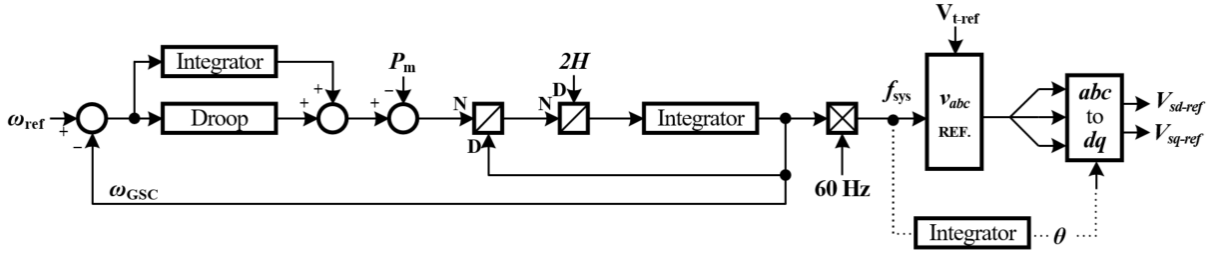

Figure 10: reference generator block of GSC

The GSC controller block is as shown in the figure below:

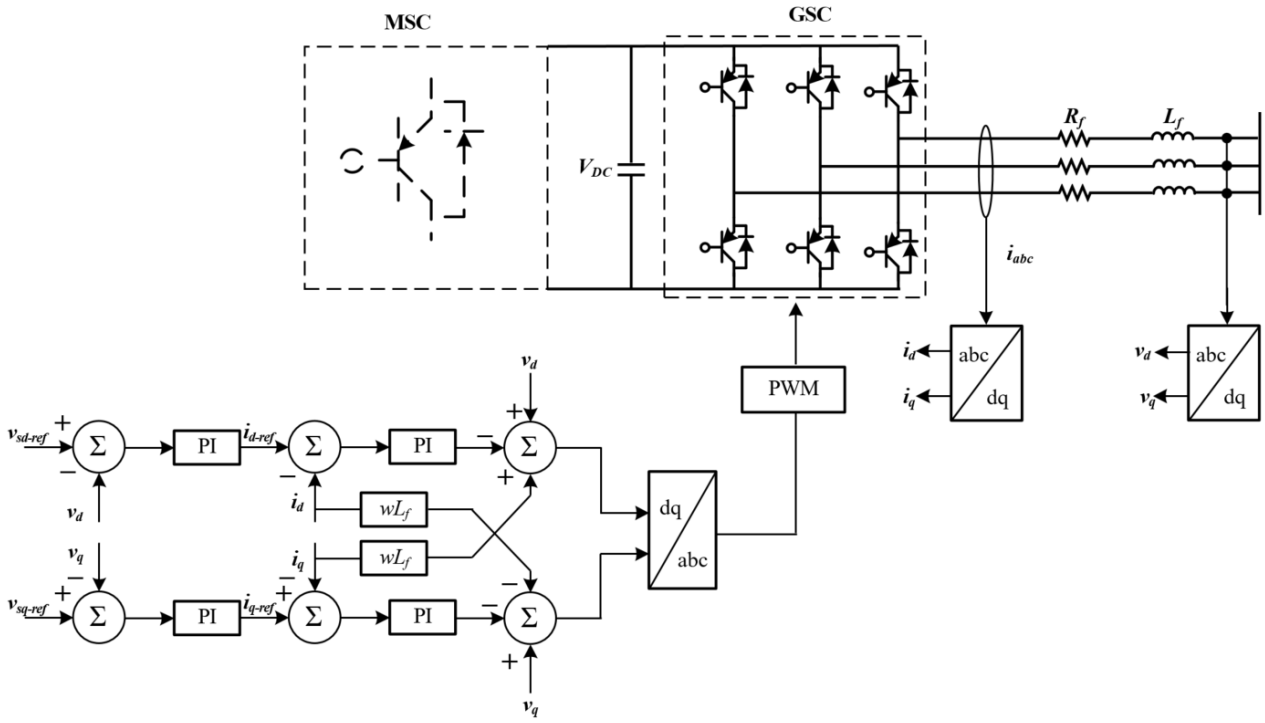

Figure 11: GSC controller of wind turbine

The outer loops regulate the stator dq-axis voltages to track the voltage references determined from the voltage reference generator, while the inner loops regulate the currents accordingly.

From figure 11 above, the voltage balance across the inductor L_f is obtained by KVL as follows:

$$\begin{bmatrix} v_a \\ v_b \\ v_c \end{bmatrix} = R_f \begin{bmatrix} i_a \\ i_b \\ i_c \end{bmatrix} + L_f \frac{d}{dt} \begin{bmatrix} i_a \\ i_b \\ i_c \end{bmatrix} + \begin{bmatrix} v_{a1} \\ v_{b1} \\ v_{c1} \end{bmatrix} \tag{20}$$

where:

L_f is the filter inductance;

R_f is the filter resistance;

v_{a1}, v_{b1}, v_{c1} are the voltages at the inverter output;

i_a, i_b, i_c are the line currents.

The vector representation of a balanced three-phase system and their equivalent vectors in a rotating dq reference frame is explained in appendix A:

Transforming the voltage equation using dq transformation in the rotating frame, we obtain the following equations:

$$v_d = v_{di} - R_f i_d - L_f \frac{di_d}{dt} + wL_f i_q \tag{21}$$

$$v_q = v_{qi} - R_f i_q - L_f \frac{di_q}{dt} - wL_f i_d \tag{22}$$

The instantaneous power in a three-phase system is given by:

$$P(t) = v_a i_a + v_b i_b + v_c i_c \tag{23}$$

Using dq transformation, the active and reactive power is given by:

$$P = \frac{3}{2}(v_d i_d + v_q i_q) \tag{24}$$

$$Q = \frac{3}{2}(v_d i_q + v_q i_d) \tag{25}$$

2.4 DC Link Modelling (Dynamics):

Traditionally, a wind turbine is modeled using detailed switching models. However, these require small integration time steps and consequently become computationally inefficient. [18]. The wind turbine dynamics can be simplified by using an average model for fast simulation and transient stability analysis. In the average model, the back-to-back converter with the PWM is replaced by controlled dependent voltage sources, as shown in Figure 12 below. Current flowing in the DC link can be calculated from the active power through the converters and the voltage at the capacitor V_{dc} as follows:

$$i_{g-dc} = \frac{P_g}{V_{dc}} \tag{26}$$

$$i_{t-dc} = \frac{P_t}{V_{dc}} \tag{27}$$

where:

i_{g-dc} is the current from the MSC;

i_{t-dc} is the current from the GSC;

P_g is the active power into the MSC;

P_t is the active power from the GSC.

V_{dc} is calculated from i_{g-dc} and i_{t-dc} by:

$$V_{dc} = \frac{1}{C}\int (i_{g-dc} - i_{t-dc})dt + V_{dc\_0} \tag{28}$$

where C is the capacitance at the DC link.

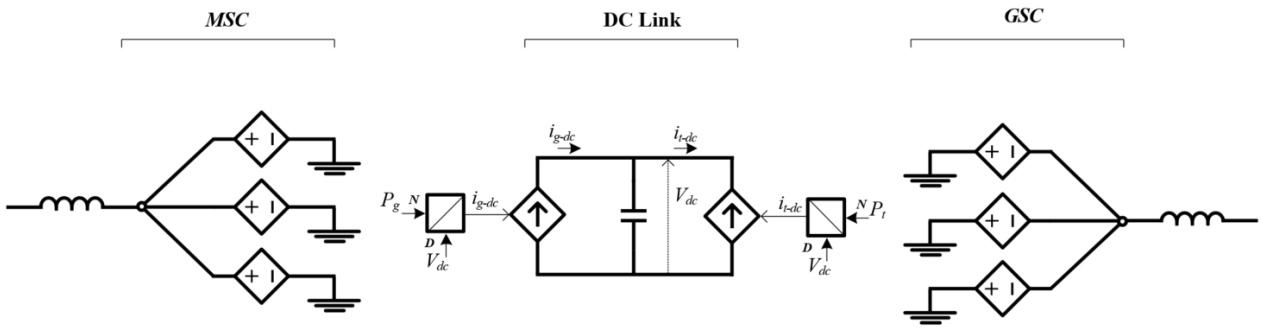

Figure 12: Generalized average model of the wind turbine.

2.5 Energy storage modeling:

Energy storage devices can be utilized to maintain the power balance of the system, hence keeping the DC link of the wind turbine at its reference value. In this thesis, BESS, FC and ELZ are employed for this purpose. The BESS is used as the main storage system because it operates with a faster transient response time than the hydrogen storage which is used as backup storage for long term energy balance and to keep the BESS operating at its optimal efficiency.

2.5.1 Battery Storage modeling:

Three types of battery models are typically reported in the literature: experimental, electrochemical, and electric circuit-based. Experimental and electrochemical models are not well suited to represent cell dynamics for state-of-charge (SOC) estimations of battery packs. However, electric circuit-based models can be useful to represent the electrical characteristics of batteries. The simplest form of the electric circuit-based battery model is an ideal voltage source with internal resistance.

Shepherd developed an equation that describes the electrochemical behavior as a function of the terminal voltage, open-circuit voltage, internal resistance, charge/discharge current, and the state of charge. The Shepherd model, however, may cause an algebraic loop problem in closed-loop simulations.

For this thesis, a generic battery model presented in [19] is implemented, which uses only the battery SOC as the state variable in order to avoid the algebraic loop problem and can accurately represent four types of battery chemistries: Lead-Acid, Lithium-Ion (Li-Ion), Nickel-Cadmium (NiCd) and Nickel-Metal-Hydride (NiMH).

The battery is modelled using a simple controlled voltage source with a constant resistance as shown in fig 13 below. The controlled voltage source is determined by the following equation:

$$E = E_0 - K\frac{Q}{Q - \int i_{batt}dt} + Aexp(-B\int i_{batt}dt) \tag{29}$$

$$V_{batt} = E - Ri_{batt} \tag{30}$$

where:

E_0 is the no-load battery voltage (V);

K is the polarization voltage (V);

Q is the battery capacity (Ah);

$\int idt$ is the charge drawn/supplied by the battery (Ah);

A is the exponential zone amplitude (V);

B is the exponential zone time constant inverse $(Ah)^{-1}$;

V_{batt} is the battery voltage (V);

R_{batt} is the battery internal resistance (Ω);

i_{batt} is the battery current (A).

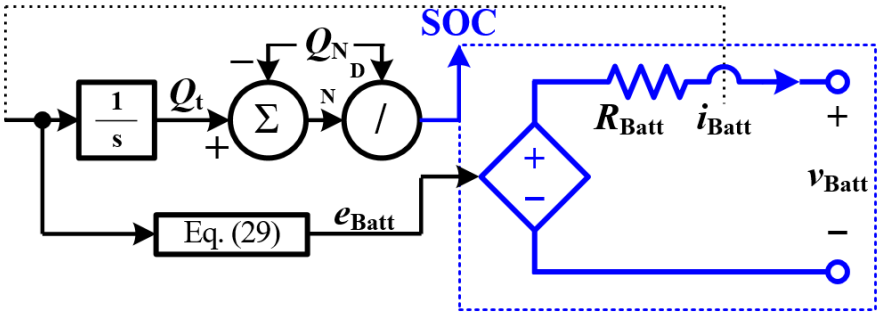

Figure 13: Battery equivalent model

The Battery SOC is calculated at every time step by:

$$SOC = \frac{Q - \int i_{batt} dt}{Q} \tag{31}$$

2.5.2. Hydrogen storage modeling:

The hydrogen system consists of an electrolyzer system to consume the surplus power while the wind power is more than the predetermined value, and a fuel cell to supply the deficit power whilst wind power is less than a predetermined value by converting hydrogen to electricity. The modeling of these components is presented as follows:

Electrolyzer modeling:

The electrolyzer consumes electric power to produce hydrogen. Water electrolysis occurs when DC current passes between two electrodes – the cathode and the anode, separated by an aqueous electrolyte with good ionic conductivity. Available electrolyzer technologies can be classified according to its electrolyte into:

- alkaline electrolyzers (AWE),
- PEM electrolyzers (PEMWE),
- Anion Exchange Membrane Electrolyzers
- solid oxide electrolyzers (SOWE)

Nowadays, only AWE and PEMWE technologies have enough maturity to find commercial units. The alkaline electrolyzer is utilized in this study due to its durability and cheapness as alkaline electrolyzers can be made of abundant and inexpensive materials.

The chemical reaction that occurs during electrolysis can be expressed as [20]:

$$H_2O_{(l)} + electrical\ energy \rightarrow H_{2_{(g)}} + \frac{1}{2}O_{2_{(g)}} \tag{32}$$

The minimum voltage required for the reaction to occur is called the reversible voltage and is derived from Gibbs free energy equation as:

$$U_{rev} = \frac{\Delta G}{nF} \tag{33}$$

where:

n is the number of moles of electrons transferred per mole of water,

F is Faraday's constant (96,485 $Cmol^{-1}$)

ΔG is given as 237$kJmol^{-1}$ which is the standard Gibbs energy for water splitting.

The voltage drop across each electrolyzer cell is the summation of the activation overvoltage and ohmic overvoltage given as [21]:

$$V_{cell} = U_{rev} + \eta_{ohmic} + \eta_{activation} \tag{34}$$

which is further expatiated below as:

$$V_{cell} = U_{rev} + {i_{elz}}/{A_{elz}}\,(r_1 + r_2 T_{elz}) + u_1 log\left(\frac{\left(t_1 + {t_2}/{T_{elz}} + {t_3}/{T^2}_{elz}\right)}{A_{elz}} i_{elz} + 1\right) \quad (35)$$

where:

A_{elz} is the cell area of the electrolyzer.

T_{elz} is the cell temperature of the electrolyzer.

r_1, r_2 are constants related to the ohmic resistance of electrolyte, Ωm^2

s is coefficient for overvoltage on electrodes, V.

t_1, t_2, t_3 are coefficients for overvoltage on electrodes, $A^{-1}m^2$

Although temperature affects the operation of the electrolyzer, in a typical set up, the time constant in the thermal domain is much larger than in the other physical domains. Therefore, a constant temperature T_{elz} can be set externally to substitute the thermal model [22].

The voltage for a number of stacked electrolyzer cells is expressed as:

$$V_{elz} = N_{elz} V_{cell} \quad (36)$$

where:

N_{elz} is the number of stacked electrolyzer cells.

While the total power consumption of the electrolyzer is given as:

$$P_{elz} = V_{elz} I_{elz} \quad (37)$$

Efficiency of Electrolyzer cell:

If all the electrical energy injected into the electrolyzer is transformed into hydrogen, the

reversible potential would be given by:

$$U_{rev} = \frac{\Delta H}{nF} \tag{38}$$

ΔH is the enthalpy of the operation, KJ.mol^{-1}. The standard enthalpy for splitting water is $\Delta H = 286KJmol^{-1}$

Thus, it is reasonable to define the electrolyzer efficiency as a ratio between the ideal voltage and the actual voltage across the cell. The electrolyzer efficiency is thus obtained as:

$$Efficiency = \frac{U_{rev}}{V_{cell}} \times 100\% \tag{39}$$

For a given temperature, an increase in hydrogen production (i.e., an increase in current density) increases the cell voltage, which consequently decreases energy efficiency. For a given current density, the energy efficiency increases with increasing cell temperature [21].

Hydrogen Production in Electrolyzer:

The electrolyzer receives current from the DC circuit to produce hydrogen at the hydrogen production rate given as below:

$$\dot{m}_{pro} = \alpha_{elz}(T_{elz}, J_{elz}) \frac{N_{elz}}{2F} I_{elz} \tag{40}$$

where the current efficiency α_{elz} also varies with the electrolyzer current density and can be described by the equation below:

$$\alpha_{elz} = \frac{\left({}^{i_{elz}}/_{A}\right)^2}{f_1 + \left({}^{i_{elz}}/_{A}\right)^2} f_2 \tag{41}$$

where f_1, f_2 and A for this study are 250mAcm^{-4}, 0.96, area of electrode (m^2) respectively [23].

Therefore, the stored hydrogen rate in the electrolyzer is obtained as:

$$\dot{m}_{elz} = \dot{m}_{pro} - \dot{m}_{out} \tag{42}$$

where $\dot{m}_{out}$ is the outlet rate controlled by the compressor.

Then the stored hydrogen quantity in the electrolzyer m_{elz} is obtained as:

$$\int m_{elz} = \int \dot{m}_{elz}\, dt + m_{elz_{(0)}} \tag{43}$$

$m_{elz_{(0)}}$ is the initial value of the stored hydrogen in electrolzyer.

The hydrogen pressure in the electrolyzer p_{elz} is:

$$p_{elz} = \frac{RT_{elz}}{V_{elz}} m_{elz} \tag{44}$$

The equivalent circuit for an electrolyzer consists of a voltage source in parallel with an equivalent series resistance (ESR) as described in the figure below:

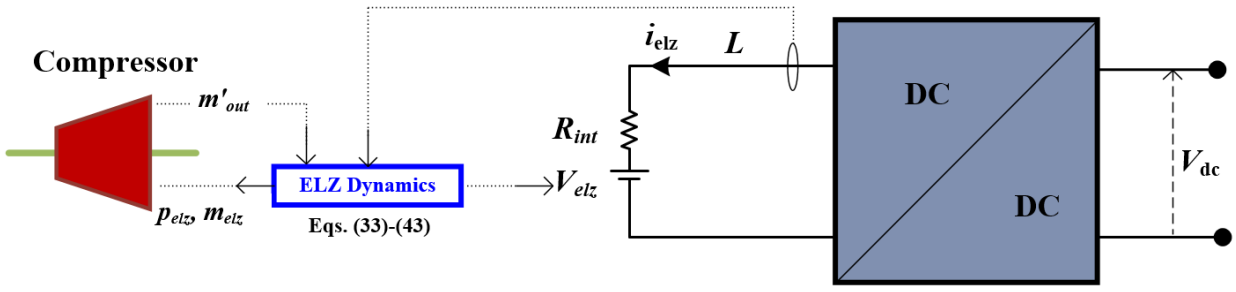

Figure 14: Equivalent circuit of the electrolyzer

The PSCAD model of the electrolyzer used in this study is shown below:

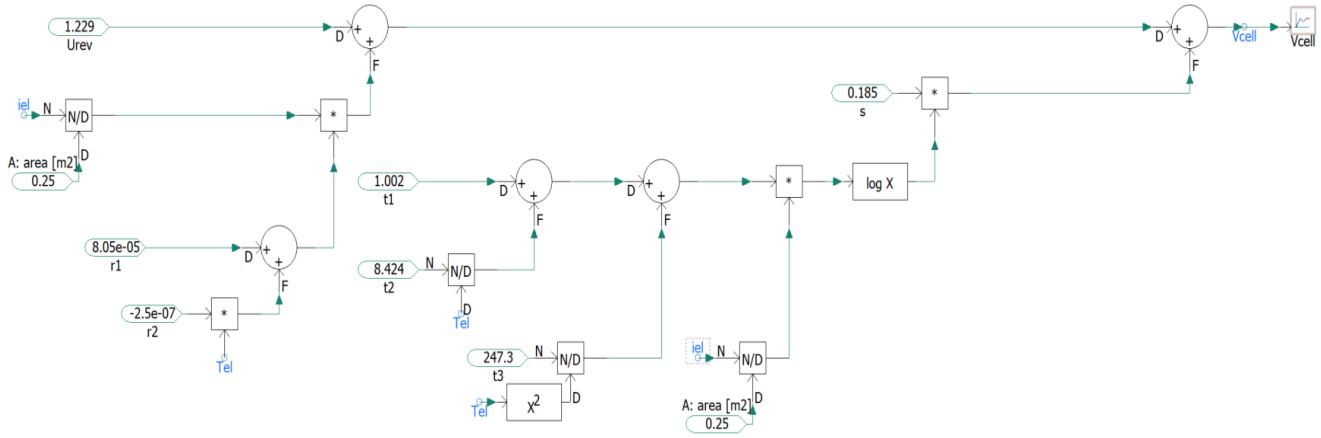

Figure 15: PSCAD model of electrolyzer cell

The figure 16 below gives the non-linear relationship between voltage and current of an electrolyzer cell across different cell temperatures:

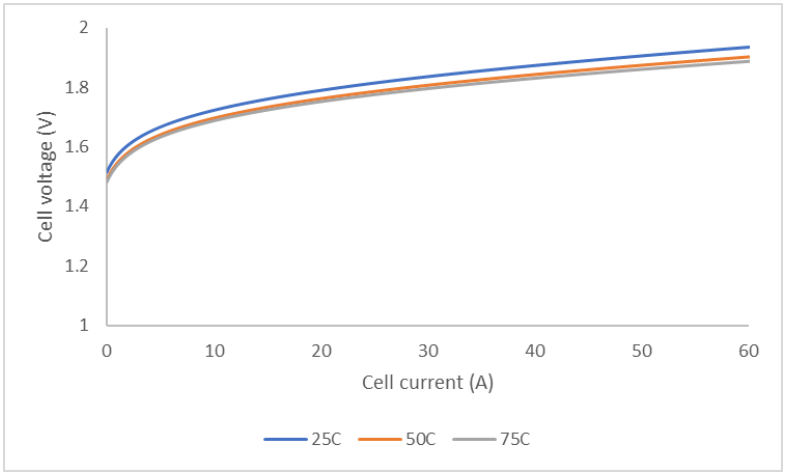

Figure 16: V-I Characteristics of an electrolyzer

Compressor and storage tank modeling:

The compressor maintains the electrolyzer pressure and drives the hydrogen from the electrolyzer to the storage tank [22].

The reference electrolyzer hydrogen quantity and the measured hydrogen quantity are as follows:

$$m_{elz\_ref} = \frac{V_{elz}}{RT_{elz}} p_{elz\_ref} \tag{45}$$

$$m_{elz\_est} = \frac{V_{elz}}{RT_{elz}} p_{elz} \tag{46}$$

The reference hydrogen quantity rate is obtained by:

$$p_{elz} = \frac{RT_{elz}}{V_{elz}} m_{elz} \tag{47}$$

$$\dot{m}_{out\_ref} = C_m(m_{elz_{ref}} - m_{elz\_est}) \tag{48}$$

Cm is a proportional gain

The desired compressor power is given as:

$$P_{comp\_ref} = \frac{w}{\alpha_{eff}} \dot{m}_{out\_ref} \tag{49}$$

where w and α_{eff} are the polytropic work and efficiency of the compressor respectively. w is given by:

$$w = \frac{kRT_{elz}}{k-1}\left[\left(\frac{p_{tank}}{p_{elz}}\right)^{(k-1/k)} - 1\right] \tag{50}$$

Therefore, outflow rate from the compressor is given as:

$$\dot{m}_{out} = \frac{\alpha_{eff}}{w} P_{comp} \tag{51}$$

The stored hydrogen rate can be expressed as:

$$\dot{m}_{tank} = \dot{m}_{out} - \dot{m}_{FC} \tag{52}$$

and the stored hydrogen in the tank can be calculated as:

$$m_{tank} = \int \dot{m}_{tank}\, dt + m_{tank_{(0)}} \tag{53}$$

where $m_{tank_{(0)}}$ is the initial value of the stored hydrogen.

The pressure in the tank can therefore by obtained as:

$$p_{tank} = \frac{RT_{tank}}{V_{tank}} m_{tank} \tag{54}$$

where T_{tank} and V_{tank} are the temperature and volume of the tank respectively.

The diagram below shows a summary of the compressor and storage tank dynamics.

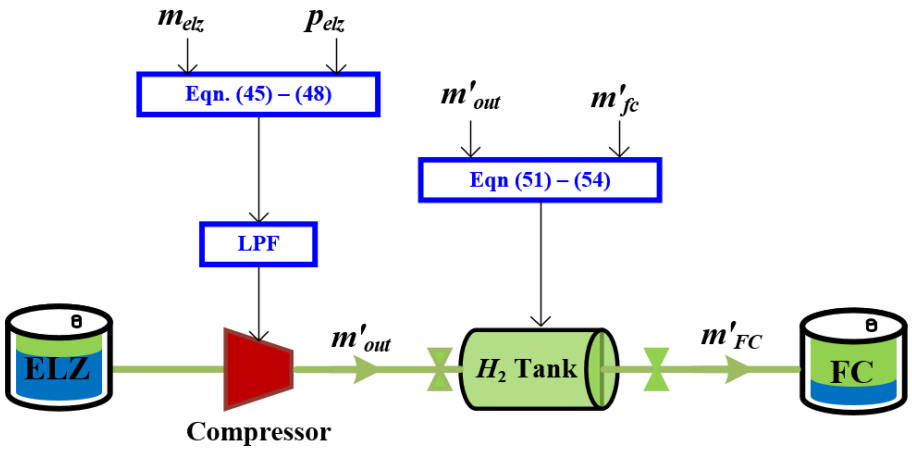

Figure 17: block of compressor and storage dynamics

Fuel Cell modeling:

Fuel Cells (FCs) are stationary electrochemical devices that generate electrical energy through chemical reactions performed on their input fuels. The behavior of a PEM FC is highly non-linear and is dependent on a range of factors such as temperature, reactant pressure, membrane

hydration, reactant concentrations and electrical load. There are various types of FCs:

- polymer electrolyte membrane FC (PEMFC),
- solid oxide FC (SOFC),
- alkaline FC, etc.

Among the different FC types, the PEMFCs are modular, scalable, and effective in high-power stand-alone power applications due to their high efficiency and thermal stability. The PEMFC model considered in this thesis is a comprehensive model that covers all dynamic aspects inside the cell.

The output voltage of the fuel cell is given as the summation of the Nernst instantaneous voltage E, the activation overvoltage, η_{act} and the ohmic overvoltage, η_{ohmic} and is expressed as follows [24]:

$$V_{cell} = E + \eta_{act} + \eta_{ohmic} \tag{55}$$

where η_{act} is a function of oxygen concentration C_{O_2} and I_{fc}, and η_{ohmic} is a function of I_{fc} and stack internal resistance R^{int}. If we assume a constant oxygen concentration and temperature, we can model the fuel cell as a multi-variable dependent voltage source that the equation can express:

$$V_{cell} = E - B_1.\ln(B_2 I_{fc}) - R^{int} i_{fc} \tag{56}$$

where the constants B1 and B2 are experimentally obtained as B_1 = 0.04777V and B_2 = 0.0136A^{-1}.

The Nernst voltage is expressed as:

$$E = N_0 \left\{ E_0 + \frac{R.T}{2F} log \left(\frac{P_{H_2}.{P_{O_2}}^{0.5}}{P_{H_2O}} \right) \right\} \quad (57)$$

where E_0, P_{H_2}, P_{O_2} and P_{H_2O} are the open cell voltage, hydrogen partial pressure, oxygen partial pressure and water partial pressure expressed as:

$$P_{H_2} = \frac{m^{'}_{FC} - 2k_r.i_{FC}}{k_{H_2}(1 + \tau_{H_2}s)} \quad (58)$$

$$P_{O_2} = \frac{(m^{'}_{FC}/r_{HO}) - 2k_r}{k_{O_2}(1 + \tau_{O_2}s)} \quad (59)$$

$$P_{H_2O} = \frac{2k_r.i_{FC}}{k_{H_2O}(1 + \tau_{H_2O}s)} \quad (60)$$

where k_r, r_{HO}, k_{H_2}, k_{H_2O}, τ_{H_2}, τ_{O_2}, τ_{H_2O} are modeling constant, hydrogen-oxygen flow ratio, hydrogen valve molar constant, oxygen valve molar constant, water valve molar constant, hydrogen time constant, oxygen time constant, and water time constant.

The K_r constant is defined by the relation between the rate of reactant of hydrogen and the fuel cell current as:

$$q^r{}_{H_2} = \frac{N_0 I}{2F} = 2K_r I_{fc} \quad (61)$$

The equivalent voltage of a number of stacked fuel cells is expressed as:

$$V_{fc} = N_{fc} V_{cell} \quad (62)$$

where:

N_{fc} is the number of stacked cells

The total electric power of the fuel cell stack is given as:

$$P_{fc} = I_{fc} V_{fc} \quad (63)$$

The equivalent electrical circuit of a PEMFC describing the above equations is as shown in

figure 18 below:

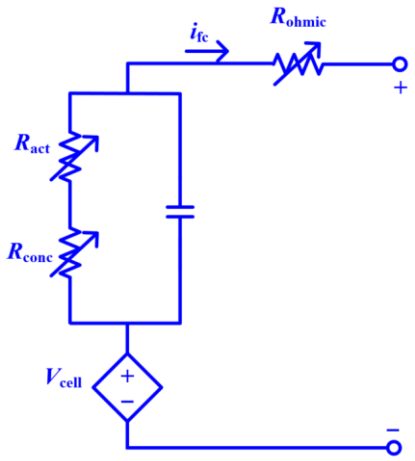

Figure 18: Equivalent electrical circuit of PEMFC

The PSCAD model of the fuel cell used in this study is shown below:

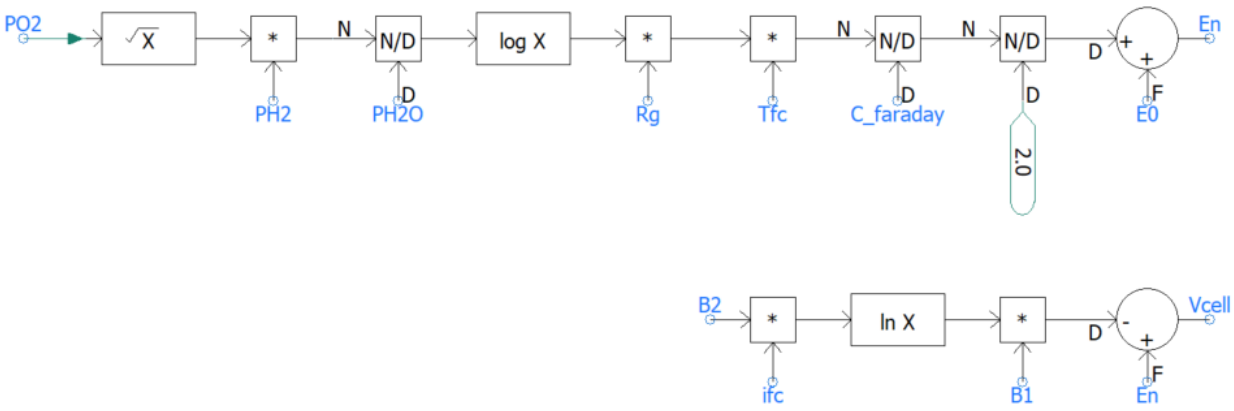

Figure 19: PSCAD model of PEMFC

Chapter 3: Coordinated Control for Power Management of Hybrid Energy System:

Hybrid energy systems are gaining ground to drive renewable energy proliferation by combining multiple energy sources and energy storage technologies to provide power, especially in standalone configurations. In standalone and isolated systems, inverter-based resources necessitate the need for efficient inverter controls to ensure a flexible and stable system operation with adequate inertia response. Two basic control technologies for utility-based inverters are: grid-following (GFL) and grid-forming (GFM). While GFL inverters control the output real and reactive power by injecting current, they cannot regulate the system frequency and voltage. Therefore, the GFL inverter must shut down if it loses a voltage or frequency source. Conversely, GFM inverters allow for direct control of the system frequency and voltage and respond faster than GFL inverters during system contingencies [25].

A hybrid energy system described in Figure 3 needs to be coordinated to achieve harmonious operation of individual subsystems, ensuring system flexibility and enhanced overall system efficiency. With the intermittent output of wind energy conversion systems, energy storage devices are identified to provide stable operation of the hybrid system. FC/ELZ combination has been in the spotlight as the subsystems and proposed for the coordination and power management of the hybrid system [24], [29], and [30]. However, the study shows that the transient response of FC and ELZ technologies is slow and do not respond sufficiently to sudden variations in the system; furthermore, it is only applicable for a GFL-hybrid system. Hence, energy storage with fast transient response i.e., supercapacitors etc. is often incorporated in most hydrogen storage designs to compensate for its slow response [26].

The previous works have been done on the application of energy storage for power management of

hybrid systems operating in GFL mode [26], [27], [28], power management strategies considering the finite capacity of the storage element and a GFM mode of a hybrid system have not been sufficiently researched. This chapter addresses these by studying the operation of the system upon simulating a dynamic model of the test system on PSCAD, and incorporating an effective power coordination control method to ensure system stability.

3.1. Power management methodology:

A proper real power management scheme is to be developed to maintain the DC bus voltage of the wind turbine. Due to variation of wind or load parameters, the DC link voltage between the MSC and GSC is affected. Thus, it is essential to maintain a constant DC-link voltage to ensure high utilization of the power converter's capability as well as for stabilizing voltage (preventing overvoltage) and maintaining power balance in the system. The active power management among the WTG, FC, ELZ, and BESS is implemented using a direct active power flow control to maintain an active power balance in the hybrid system. The figure 20 below shows the power flow demonstrating the contributions of the WTG, FC, ELZ and BESS in maintaining the DC link voltage of the system.

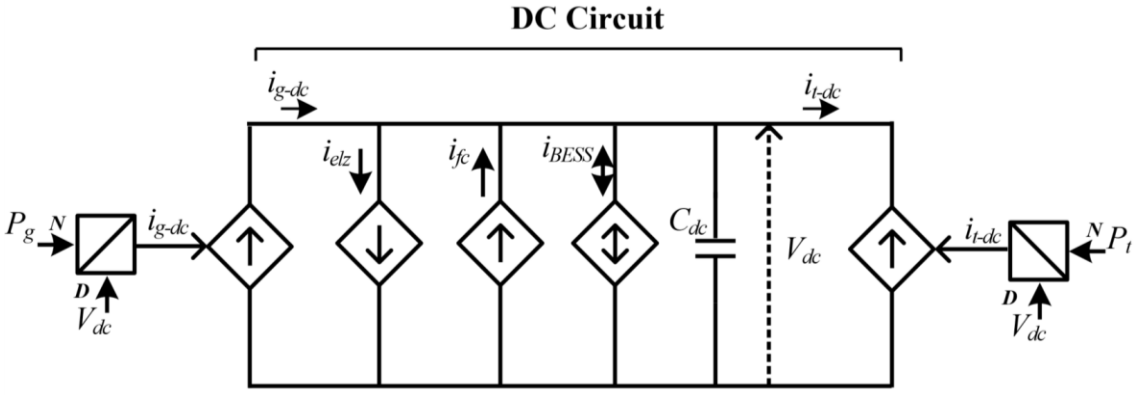

Figure 20: Wind turbine DC circuit

From the above figure, to keep the DC link voltage constant, the following equation should be met.

$$i_{g-dc} + i_{fc} - i_{elz} \pm i_{BESS} - i_{t-dc} = 0 \quad (64)$$

where:

i_{g-dc} is the current of the WTG,

i_{fc} is the fuel cell current.

i_{elz} is the electrolyzer current.

i_{BESS} is the battery current.

i_{t-dc} is the current of the GSC inverter.

$i_{t\text{-}dc}$ varies according to the system load since the GSC is being operated in GFM mode. Hence, $i_{t\text{-}dc}$ can be met by controlling i_{g-dc}, i_{fc}, i_{elz} and i_{BESS}.

To manage the hybrid system accordingly, the system generates operating points based on the wind and load conditions and the limitations of each subsystem. These limitations include the BESS state of charge (SOC_{max} and SOC_{min}), which are selected as 40% and 80% in this thesis, the maximum charging and discharging power of the BESS (P_{BESS_max}), the maximum power of the FC (P_{FC_max} and P_{FC_min}) for operation in the ohmic region, the maximum and minimum power consumption by the EZ (P_{EZ_max} and P_{EZ_min}) and the maximum pressure of the hydrogen storage tank. However, in this thesis, it is assumed that there are no storage limitations for the hydrogen system as multiple storage tanks can be located on the site ensuring continuous

operation of the hydrogen storage system. The operation of the hydrogen storage system will be studied regardless.

Since the WECS works with a maximum power point tracking strategy, the power generated by the wind turbine depends on wind at the WECS. During over-generation by the WTG or reduction in system load, the power output of the WTG P_g is greater than the load demand P_t; thus, the excess power is consumed by the BESS and the ELZ as follows:

$$P_{Ex} = P_t - P_g = -(P_{ELZ} + P_{BESS}) \tag{65}$$

If this excess power is greater than the maximum power capacity of the BESS and ELZ such that the BESS and ELZ are not able to operate, the pitch angle controller of the WTG is to be activated to curtail the excess power.

Also, during under-generation by the WTG or increase in system load, the power output of the WTG P_g is less than that of the load demand Pt. Thus, the deficit power is supplied by the BESS and the FC as follows:

$$P_{def} = P_g - P_t = P_{FC} + P_{BESS} \tag{66}$$

Since the FC and ELZ are not able to deal with rapid load variation because of the relatively slow chemical reaction process involved, the BESS is made to operate instantaneously at load or supply changes due to its faster transient response than the FC and ELZ systems. However, the FC and ELZ act as a backup to the BESS, ensuring an extended lifespan of the BESS.

Figure 21 shows the flowchart of the active power management scheme employed in this paper. The power management control scheme reads the power from the wind turbine, the GSC, as well as the DC link voltage, the battery SOC and the pressure in the hydrogen storage tank. The controller

compares the dc link voltage with a predetermined reference value to determine the error signal accordingly.

If the error signal is less than zero, it implies that the system is operating in power deficit mode. Hence, the control scheme activates the controller of the BESS or FC subsystem to discharge the battery or turn ON the fuel cell depending on battery SOC or the pressure in the hydrogen storage tank. Because of the faster response of the battery to transient conditions, the battery is turned ON, while the FC is turned ON when the battery is discharged to its lower SOC limit. If the SOC reaches its lower limit, the FC is turned ON to convert hydrogen to supply the deficit power required by the system and charge the battery accordingly. In this thesis, it is assumed that there is continuous supply of hydrogen to the FC.

Similarly, if the error signal is greater than zero, it implies the system is operating in excess power mode. Hence, the control scheme activates the controller of the BESS or ELZ subsystem to charge the battery or turn ON the electrolyzer depending on the battery SOC or the pressure in the hydrogen storage tank. Because of the faster response of the battery to transient conditions, the battery is turned ON, while the ELZ is turned ON when the battery is charged to its upper SOC limit. If the SOC reaches its upper limit, the ELZ is turned ON to generate hydrogen with the excess power supplied by the wind turbine. In a case where the storage tank is full and the battery SOC has reached its upper limit, the pitch controller of the WTG may be activated to regulate the power output of the wind turbine, however, as mentioned, there is assumed to be no limitation on the capacity of the storage tank.

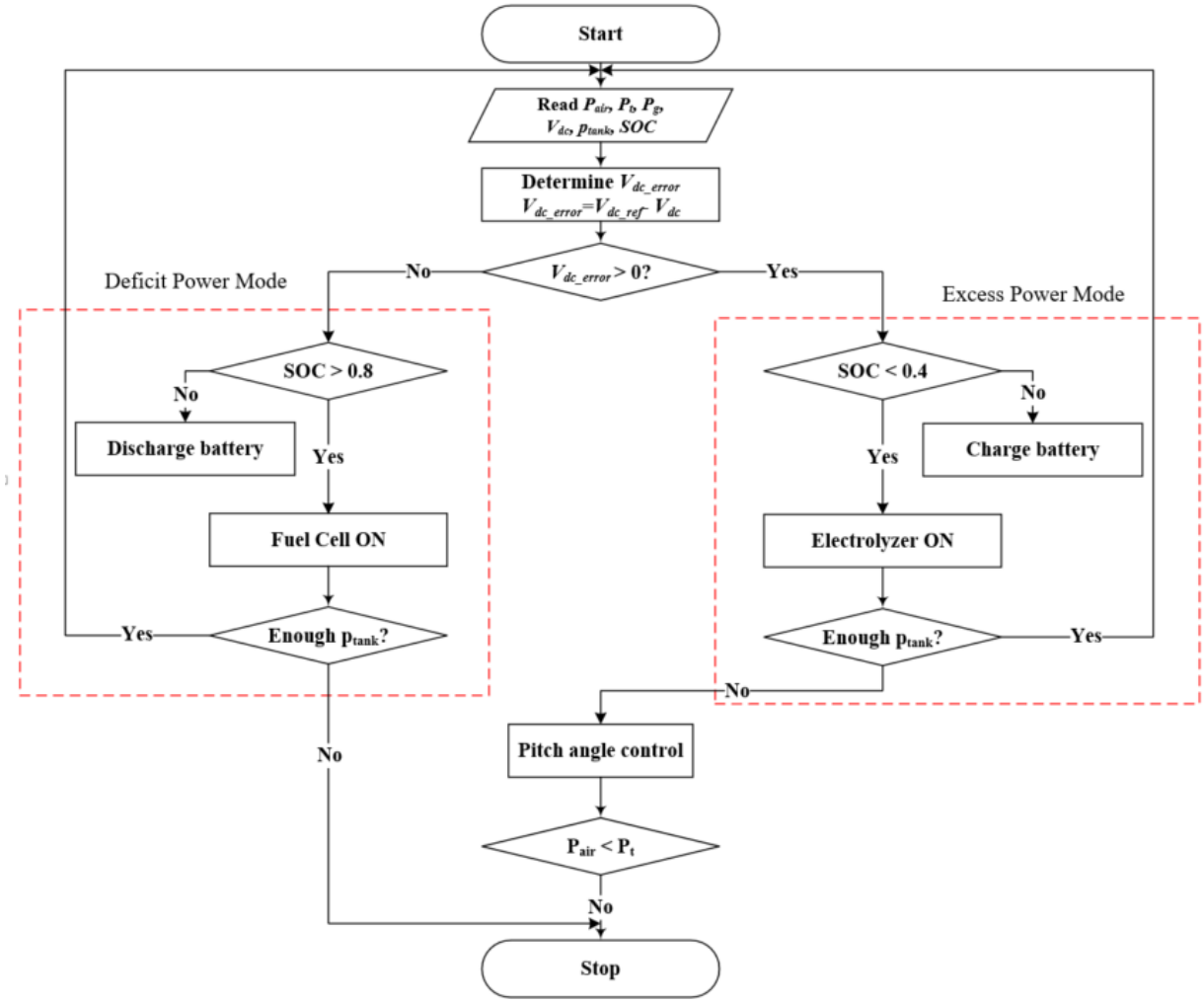

Figure 21: Flowchart of active power management system

3.2. Controller modelling:

Buck, boost, and buck-boost converters are utilized for voltage regulation and control of each storage unit. The operation of each controller is described as follows:

3.2.1 FC Boost converter controller modelling:

The boost converter regulates the power generated by the FC. This adjustment is achieved by regulating the DC link voltage according to a reference voltage $V_{dc\_ref.}$ Figure 22 below shows

the controller model for the fuel cell boost converter [29].

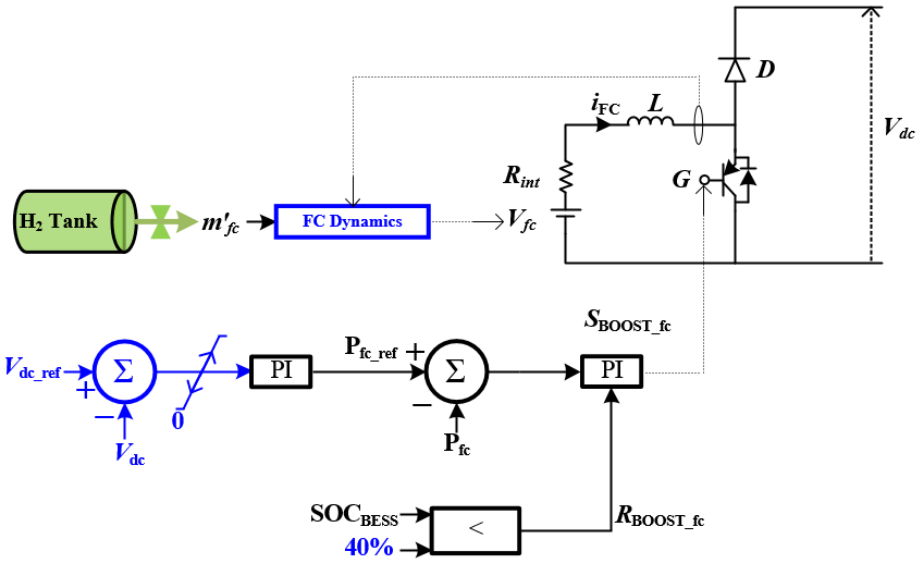

Figure 22: FC boost converter model

From the above figure, the controller is switched ON or OFF by comparing the SOC of the BESS to the set lower limit of the BESS (40%).

The control scheme is composed of two cascaded loops. The outer loop regulates the dc-link voltage and provides the reference signal for the inner control loop. The reference signal is compared with the FC power in the inner control loop and passed through a PI controller, applied to the boost converter.

3.2.2. ELZ Buck converter controller modelling:

The buck converter regulates the power supplied to the electrolyzer. This is achieved by regulating the DC link voltage according to a reference voltage V_{dc_ref}. Figure 23 below shows the controller model for the electrolyzer buck converter.

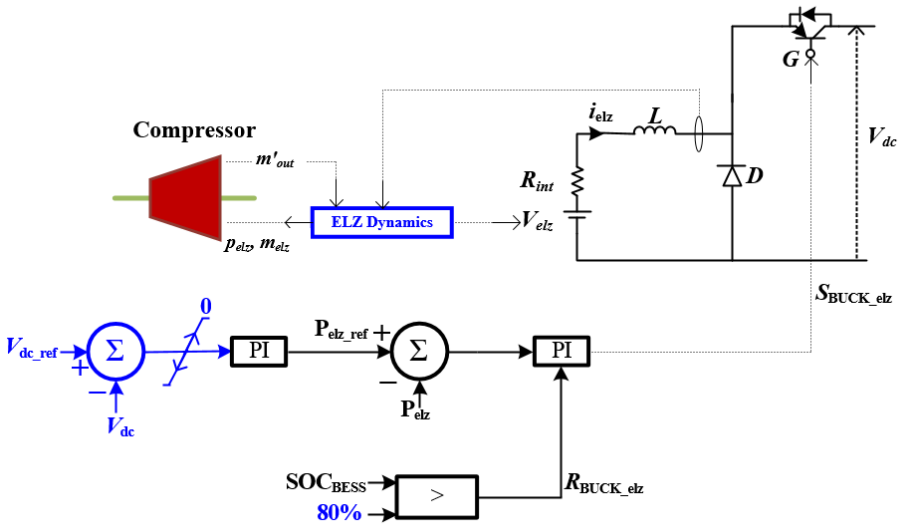

Figure 23: ELZ buck converter model

From the above figure, the controller is switched ON or OFF by comparing the SOC of the BESS to the set upper limit of the BESS (80%).

Similarly, the control scheme is composed of two cascaded loops. The outer loop regulates the dc-link voltage and provides the reference signal for the inner control loop. The reference signal is compared with the ELZ power in the inner control loop and passed through a PI controller, applied to the buck converter.

3.2.3. BESS Buck-Boost converter controller modelling:

The buck-boost converter regulates the power supplied to or generated by the battery. This is achieved by regulating the DC link voltage according to a reference voltage V_{dc_ref}. The output control loop produces a reference signal that determines the mode of operation of the controller (i.e., charging or discharging mode). When the reference signal P_{BESS_ref} is less than zero, the buck converter is operated to charge the battery; If P_{BESS_ref} is greater than zero, the boost converter is operated to discharge the battery. The BESS can be operated only if the State of Charge (SOC) of the battery is between 40% and 80%. Figure 24 shows the controller model

for the battery buck-boost converter.

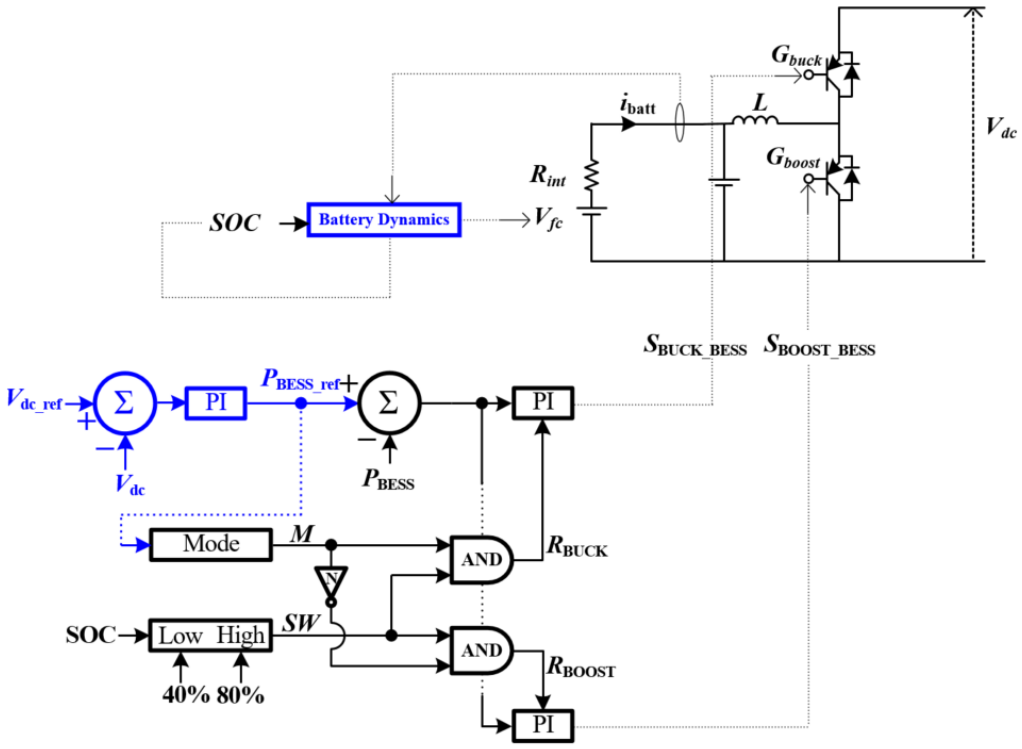

Figure 24: Battery buck-boost converter controller

Chapter 4: Simulations case studies and results:

The hybrid energy system shown in figure 3 was simulated using PSCAD/EMTDC. For simulation cases, two scenarios are considered: wind speed variation and system load variation. The system is a 5MW rated GFM-WTG with a rated wind speed of 12m/s.

Assuming minimum power from WTG in adverse conditions as 20% of its rated capacity, a 4-MW BESS will be able to supply the deficit of maximum demand. Additionally, the FC is sized to account for the no-load condition; therefore, a 5-MW PEM FC was selected. The ratings of other components are selected as 5MW each.

The changes in the loads and wind speed are represented by step changes to simulate V_{dc} variation cases and observe the response in the hybrid energy system. The dynamic model of the system, as discussed in the previous sections, is developed in PSCAD/EMTDC to test the proposed scheme under the cases

Case 1: Performance under wind speed increase.

Figure 25 shows the results for Case 1 where the wind turbine speed increases from 10 to 12m/s at t = 40s as seen in figure 25a. The load remains constant at 2.89MW. The initial battery state of charge is set as 70%. From figure 25b, there is a delay between the change in wind speed and the PMSG output power. This delay is introduced to the WECS because of the realistic two-mass model of the wind turbine. Also, due to the increase in wind speed, there is an imbalance between the generator power P_g and the terminal power P_t. Figure 25b shows the power flow between the WTG and BESS, ELZ and FC. It is seen that the BESS is activated to operate in charging, thereby absorbing the excess active power generated by the WTG since the battery SOC is within its operational limits. Likewise, the ELZ is turned off. The active power variation causes a temporary swell in V_{dc} (figure 25c) which is mitigated by the charging action of the BESS.

With the wind speed increase, the system frequency does not change because the load is fixed to 2.89MW, as shown in figure 25d. Similarly, the output voltage at the point of common coupling remains constant at 0.69KV, as seen in figure 25e. It is therefore observed that the fluctuation in wind speed does not majorly affect the output a.c. voltage unlike with load variation where the load is connected to the inverter.

The battery SOC is shown in figure 25f. It is seen that the charging action of the battery causes a rise in the SOC of the battery.

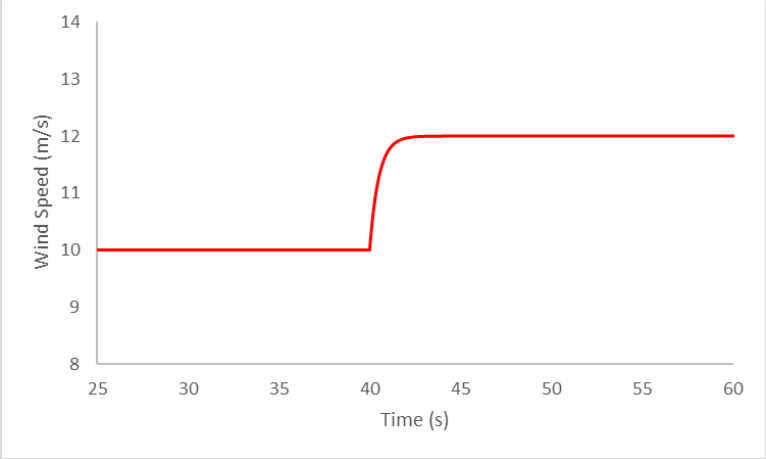

Figure 25a: wind speed

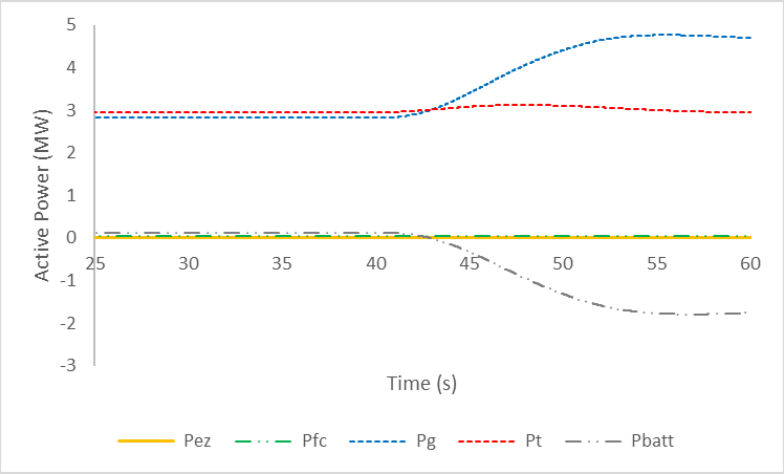

Figure 25b: Active powers from generator, ELZ, BESS, FC and GSC

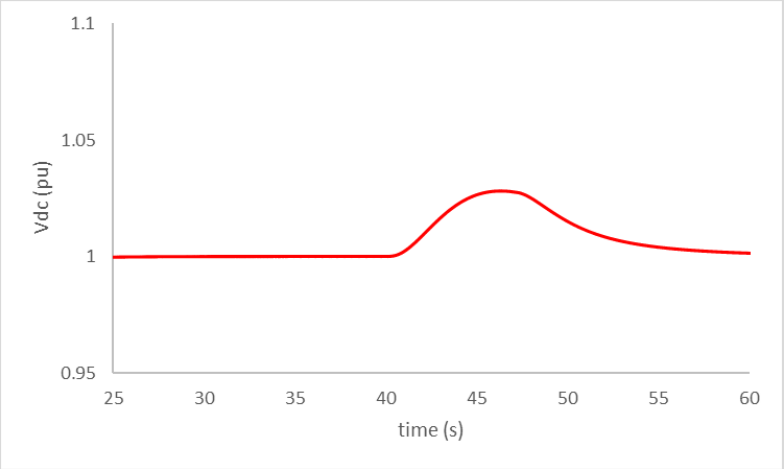

Figure 25c: DC link voltage

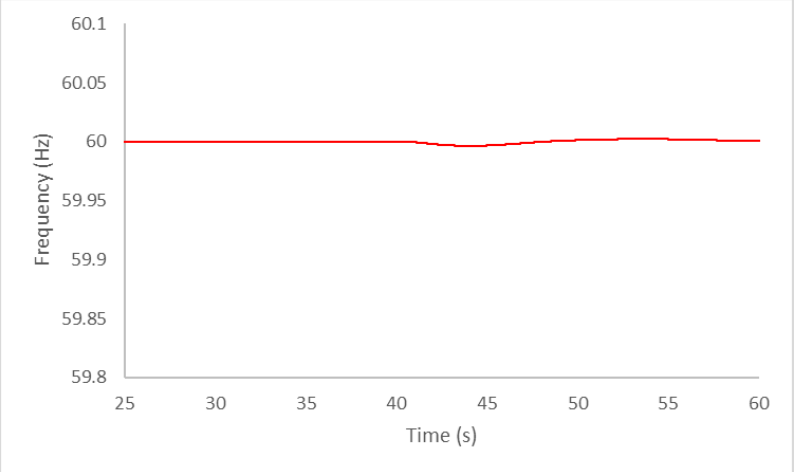

Figure 25d: System frequency

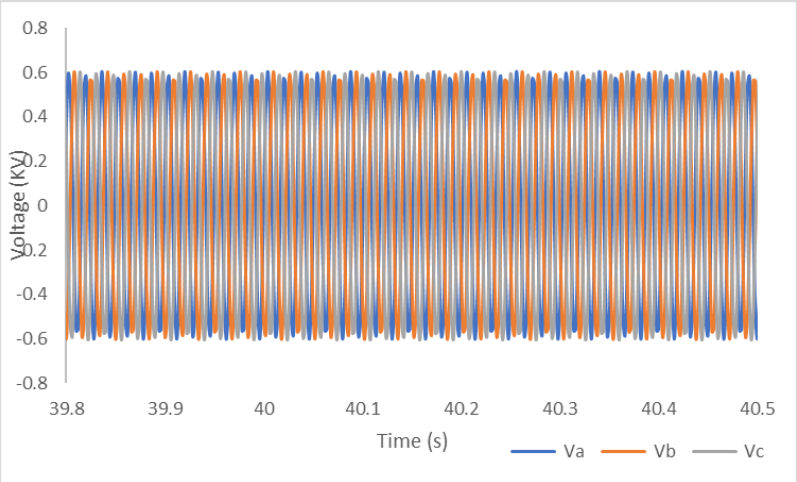

Figure 25e: Instantaneous voltage at PCC

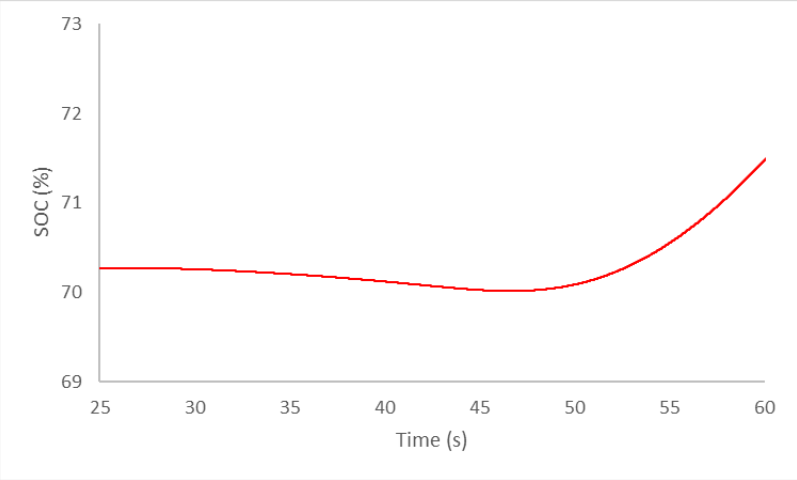

Figure 25f: Battery SOC

Performance of hydrogen storage under wind speed increase.

Previously, the FC and ELZ are warmed up and kept in standby mode so that they can quickly follow the control command when prompted. Due to the dynamics of the hydrogen storage system, a simple first-order system with time constant 5 s is assumed as a fuel regulation block for the hydrogen storage system to simulate its response [30].

To demonstrate the operation of the hydrogen storage system for this case, consider the event when

the battery SOC exceeds SOC_{BESS_max} at 60s. Therefore, the initial SOC of the BESS is set to be close to 80% so that the BESS will attain the SOC limit due to charging. In this case, the BESS is turned OFF and the ELZ is switched ON to absorb the surplus power as shown in figure 25g. Therefore, the battery power begins to reduce until it returns to zero. The DC link voltage is still maintained at its reference value as shown in figure 25h, although there is a brief overshoot at the point of switching which is mitigated by the action of the ELZ. The dynamics of the storage tank is shown in figure 25i. It is seen that the pressure in the hydrogen tank begins to increase as the ELZ is turned on to absorb excess power generated by the wind turbine.

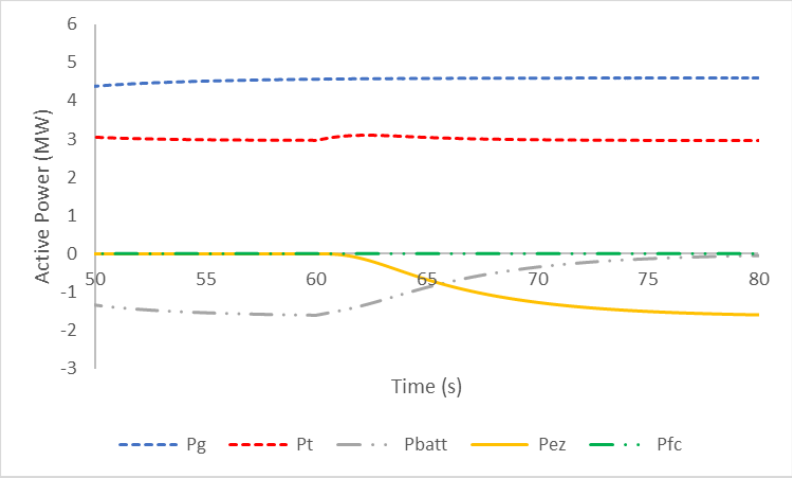

Figure 25g: Active powers from generator, ELZ, BESS, FC and GSC

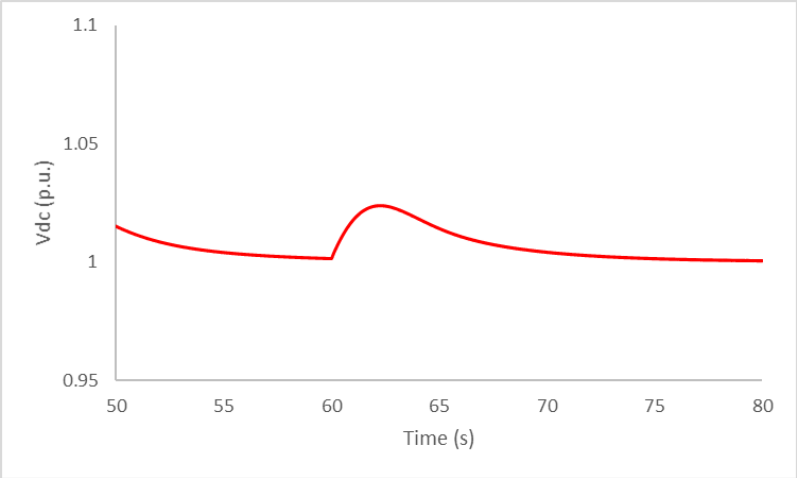

Figure 25h: DC link voltage

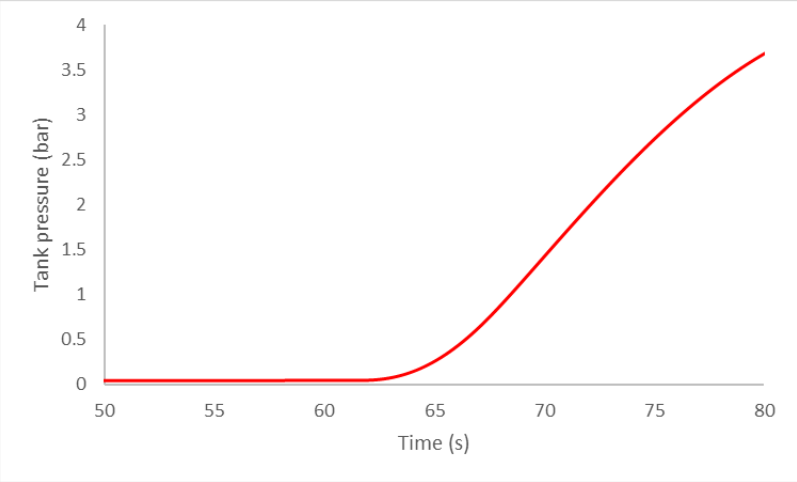

Figure 25i: Storage tank pressure

Case 2: Performance under wind speed decrease.

Figure 26 shows the results for Case 2 where the wind turbine speed decreases from 12m/s to 9m/s at t = 40s, as seen in figure 26a. The load remains constant at 4.7MW. The initial battery state of charge is set as 70%. From figure 26b, Also, due to the decrease in wind speed, there is an imbalance between the generator power P_g and the terminal power P_t. Figure 26b shows the power flow between the WTG and BESS, ELZ and FC. It is seen that the BESS is activated to operate in discharging, thereby supplying the deficit active power needed by the WTG since the battery SOC is within its

operational limits. Likewise, the FC is turned OFF. The active power variation causes a temporary dip in V_{dc} (figure 26c) which is mitigated by the discharging action of the BESS.

With the wind speed decrease, the system frequency does not change because the load is fixed to 4.7 MW, as shown in figure 26d. Similarly, the output voltage at the point of common coupling remains constant at 0.69KV.

The battery SOC is shown in figure 26e. It is seen that the discharging action of the battery causes a fall in the SOC of the battery.

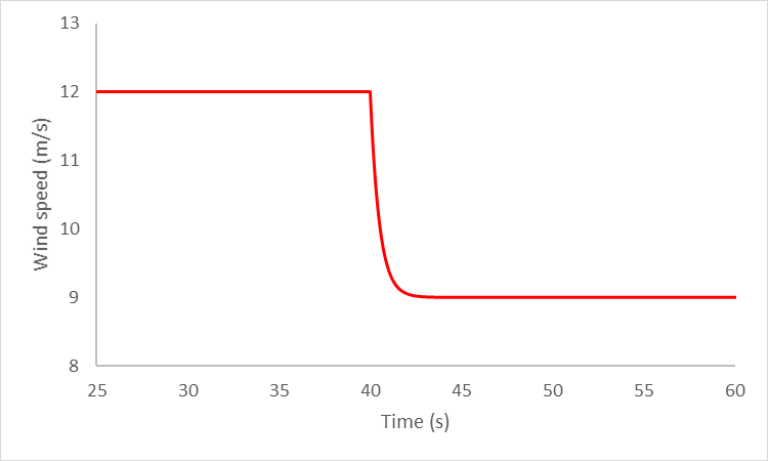

Figure 26a: wind speed

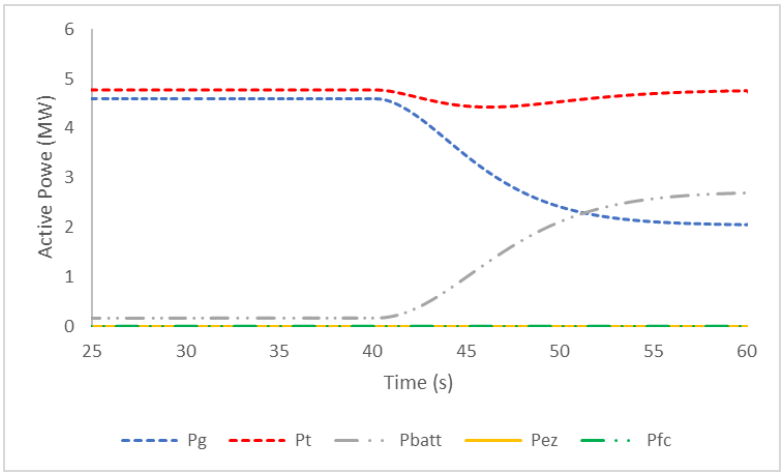

Figure 26b: Active powers from generator, ELZ, BESS, FC and GSC

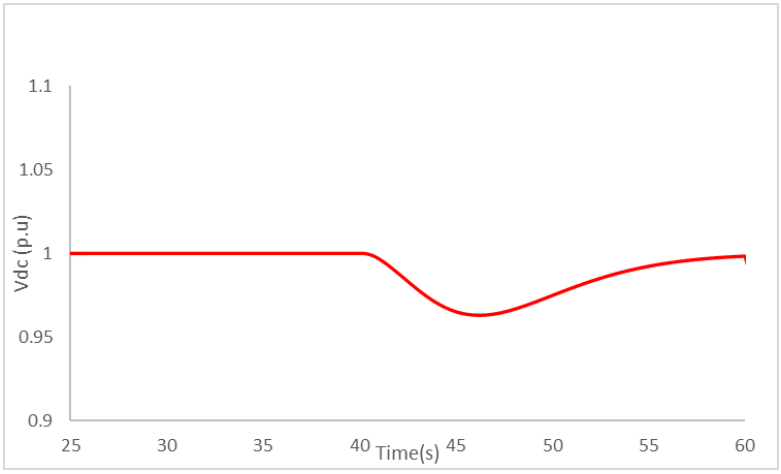

Figure 26c: DC link voltage

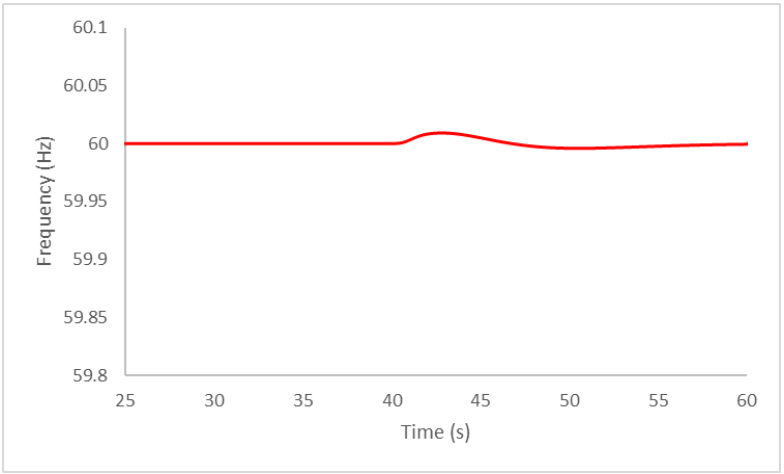

Figure 26d: System frequency

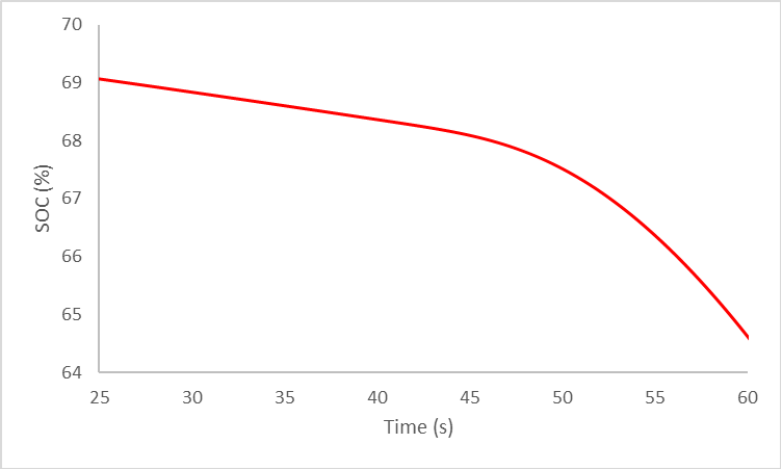

Figure 26e: Battery SOC

Performance of hydrogen storage under wind speed decrease:

To demonstrate the operation of the hydrogen storage system for this case, consider the event when the battery SOC falls below SOC_{BESS_min} at 60s as the wind speed is decreased from 12m/s to 10m/s. The generated power from the wind turbine with wind speed of 10m/s is 2.89 MW. However, the load demand is set at 4.7MW. Therefore, the initial SOC of the BESS is set to be close to 40% so that the BESS will attain the SOC limit due to discharging.

In this case, the BESS is turned OFF and the FC is switched ON to supply the deficit power, as shown in figure 26f. Therefore, the battery power begins to reduce until it returns to zero. The DC link voltage is still maintained at reference value as shown in figure 26g, although there is a brief dip in the DC voltage at the point of switching which is mitigated by the action of the FC. The FC also supplies current to charge the battery.

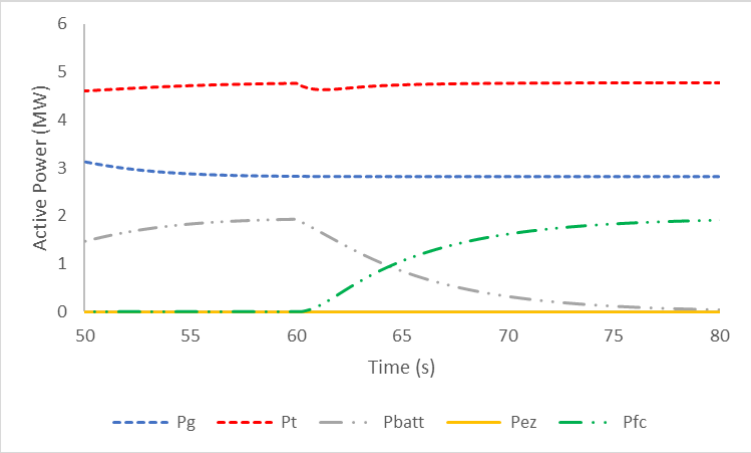

Figure 26f: Active powers from generator, ELZ, BESS, FC and GSC

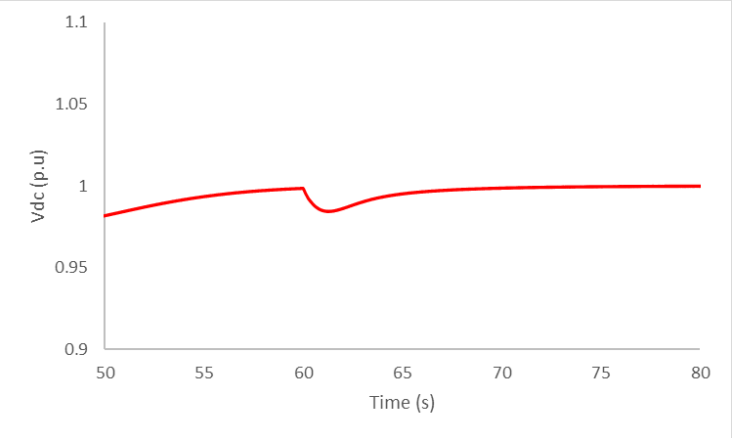

Figure 26g: DC link voltage

Case 3: Performance under load increase.

Figure 27 shows the results for Case 3, where an additional load of 1MW is added to the network at 60s, making the total load demand 3.89MW, while the wind speed remains at 10m/s. With the load increase, the system frequency decreases for a while, as shown in figure 27b, and P_{BESS} increases to meet the system load as shown in figure 27b. Thus, the sudden power increment at the terminal causes a rapid decrease in V_{dc}, as shown in figure 27c, while the P_{BESS} supplies power to stabilize V_{dc}. There is a temporary variation in the PCC voltage which decreases for a while as a result of the

increased load connected to the GSC inverter as seen in figure 26d, which is as a result of the inverter and the action of the GSC.

The initial battery SOC shown in figure 27e, is set at 70% for this simulation. Therefore, the battery controller is activated for voltage regulation, since it is within its SOC operational limits while the FC is turned off.

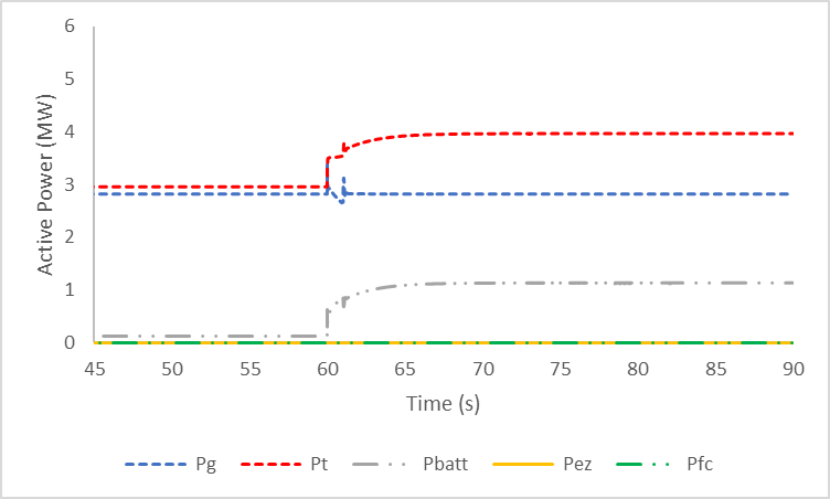

Figure 27a: Active powers from generator, electrolyzer, battery, fuel cell and GSC

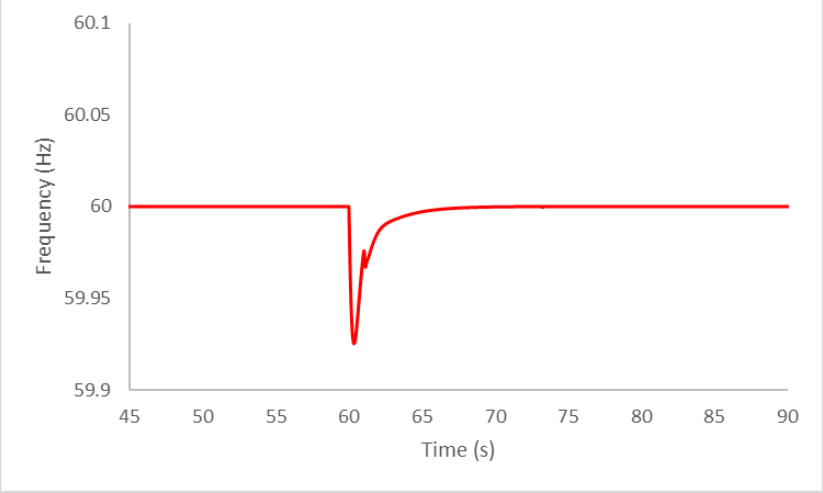

Figure 27b: system frequency

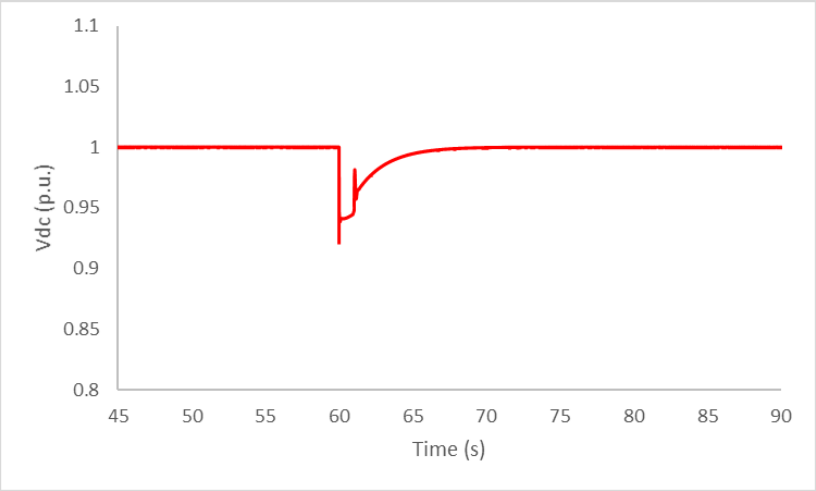

Figure 27c: DC link voltage

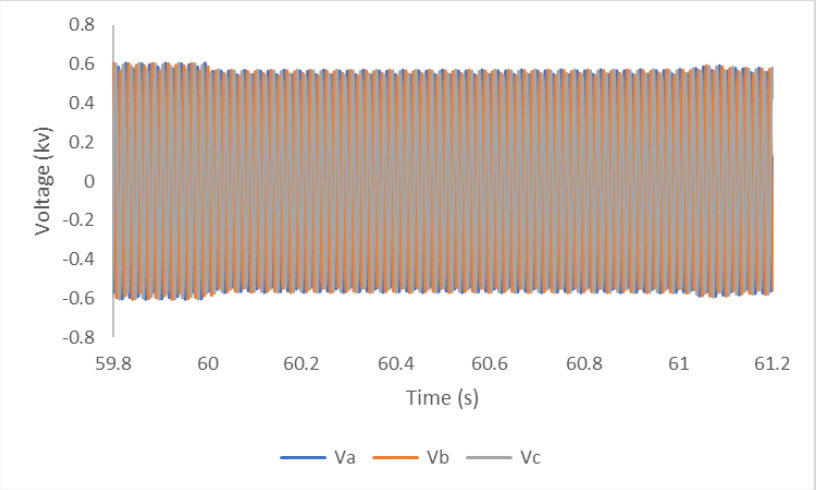

Figure 27d: Instantaneous voltage at PCC

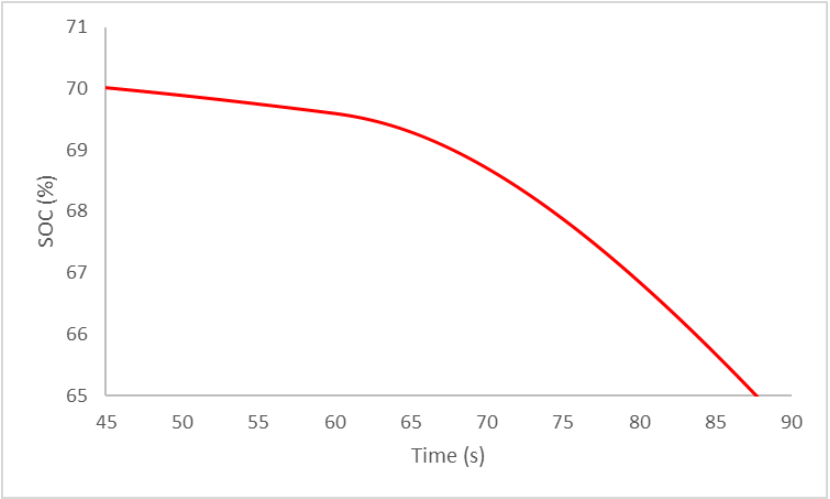

Figure 27e: Battery SOC

Case 4: Performance under load decrease.

Figure 28 shows the results for Case 4, where the load demand drops from 3.89MW to 2.50MW, while the wind speed remains constant at 11m/s. With the load decrease, the system frequency increases for a while, as shown in figure 28b, and P_{BESS} is charged to absorb the surplus power as shown in figure 28b. Thus, the sudden power decrement at the terminal causes a rapid swell in V_{dc} as shown in figure 28c, while the P_{BESS} absorbs power to stabilize V_{dc}. There is a temporary variation in the PCC voltage which increases for a while as a result of the decreased load connected to the GSC inverter as seen in figure 28d which is as a result of the inverter and the action of the GSC

The initial battery is set at 70% for this simulation. Therefore, the battery controller is activated for voltage regulation since it is within its SOC operational limits while the FC is turned off.

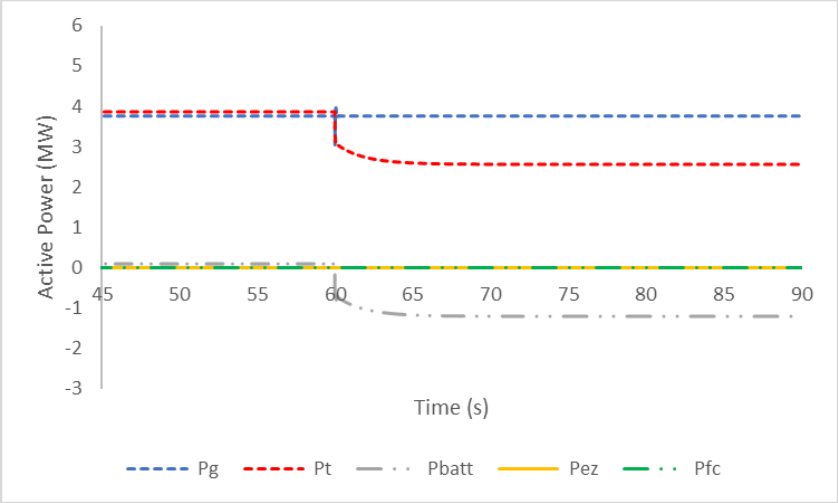

Figure 28a: Active powers from generator, electrolyzer, battery, fuel cell and GSC

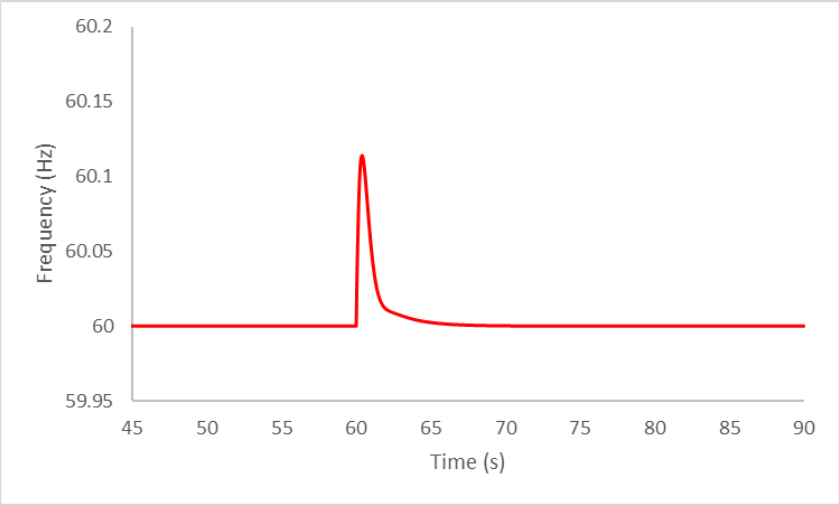

Figure 28b: System frequency

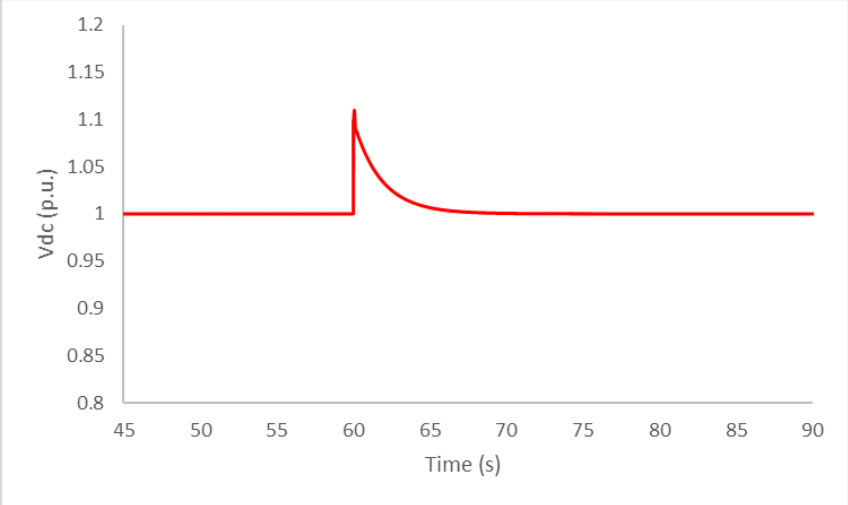

Figure 28c: DC link voltage

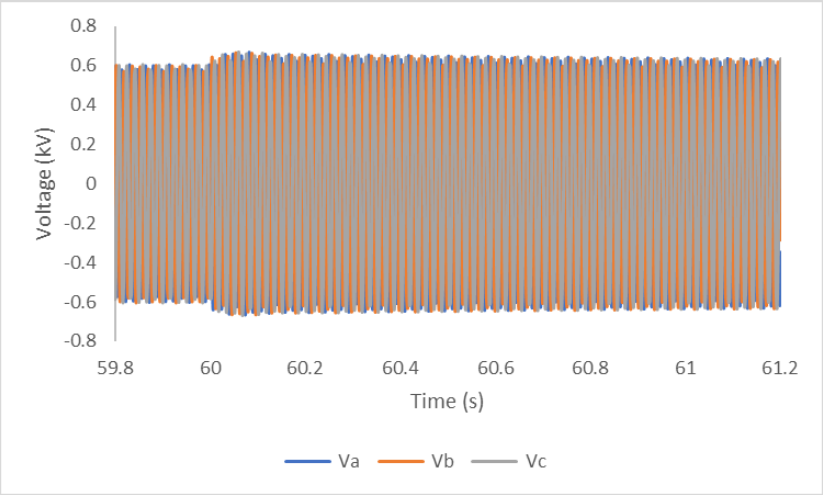

Figure 28d: Instantaneous voltage at PCC

Case 5: Performance under sudden load variation: frequency response

Consider the case where the BESS SOC falls below the lower threshold and a sudden load increase from 2.8MW to 3.8MW occurs at 30s with a wind speed of 10m/s. Although the FC is activated to supply deficit power, a co-ordination method can be created that checks the frequency of the system and compares to a threshold frequency (set at 59.95Hz). If the frequency falls below this threshold, the BESS is activated as an emergency measure to provide additional power by discharging to supply the deficit transient power as the time constant for the hydrogen storage system is larger than that of the battery which has an immediate response. Thus, the frequency nadir is greatly reduced. Figure 29a shows the results for this case. It is seen from the figure below that the BESS helps to arrest the frequency drop accordingly. The DC link voltage response is displayed in figure 29b.

Similarly, consider the case where the BESS SOC rises above the upper threshold and a sudden load decrease from 3.8MW to 2.8MW occurs at 60s with a wind speed of 11m/s. The co-ordination control method checks the frequency of the system, and compares to a threshold frequency (set at 60.05Hz). If the frequency rises above this threshold, the BESS is activated as an emergency measure

to absorb the excess power by charging for the duration of the transient period as the time constant of the hydrogen storage system is larger than that of the battery. Therefore, the BESS is able to check the frequency nadir as shown in figure 29c below.

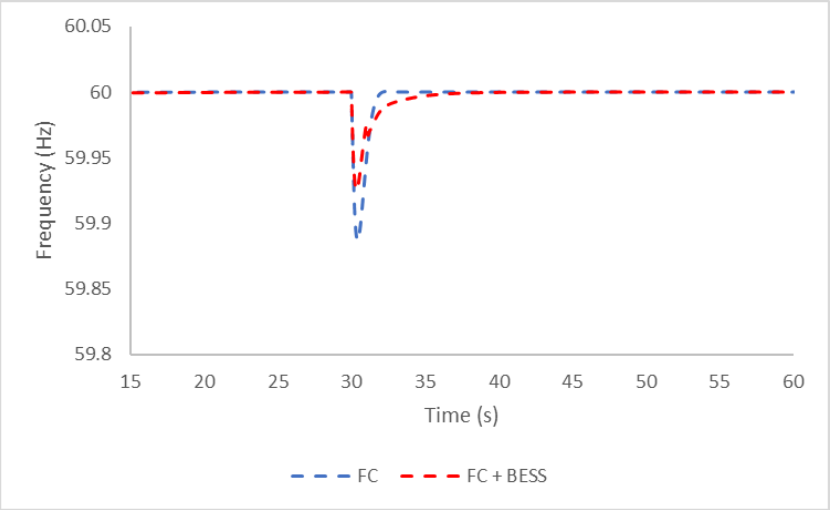

Figure 29a: System frequency: load increase

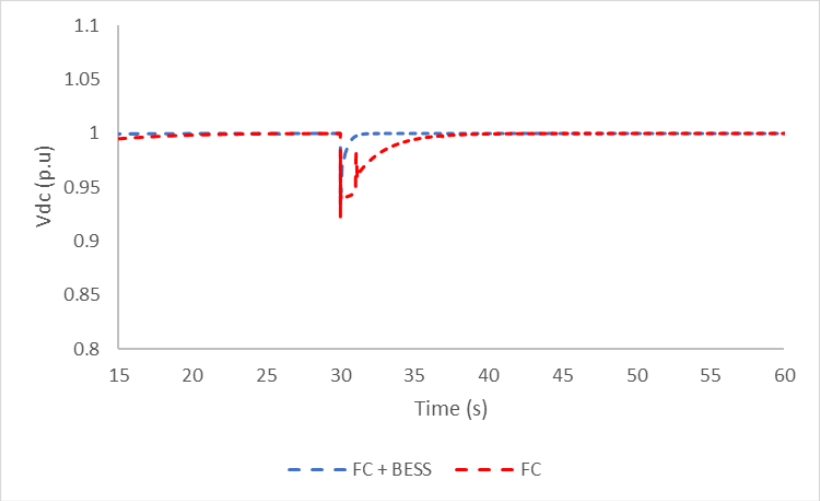

Figure 29b: DC link voltage: load increase

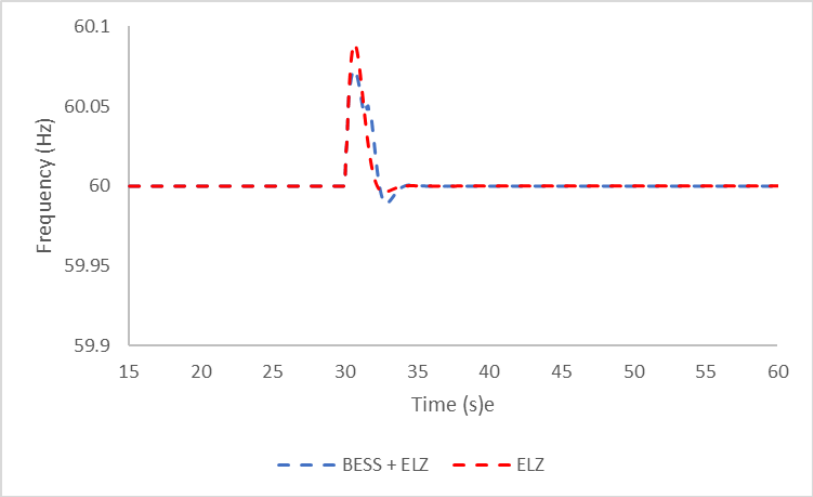

Figure 29c: System frequency: load decrease

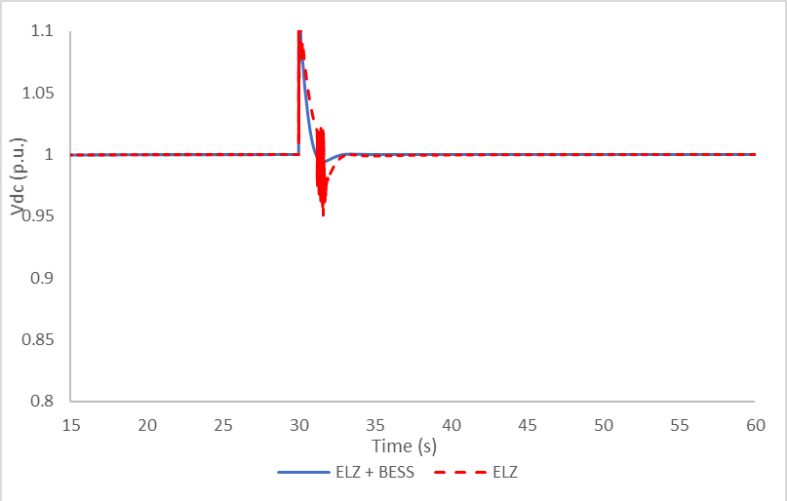

Figure 29d: DC link voltage: load decrease.

Table 1: Summary of frequency response of system for load variation.

Load Increase	**BESS + FC**	**FC**
Frequency (Hz)	59.9253	59.8869
Load decrease	**BESS + ELZ**	**ELZ**
Frequency (Hz)	60.0726	60.0900

Summary of simulation case studies:

In summary, the system has been tested under varying wind and load conditions. In each case, the battery and/or FC and ELZ is operated to keep the DC link voltage constant ensuring the stability of the system as demonstrated in the figures above.

During overgeneration/load decrease, the BESS or ELZ is activated to absorb excess power depending on the SOC of the BESS. There is a temporary swell in the DC link voltage which is immediately mitigated by the energy storage device. Also, during under generation/ load decrease, the BESS or FC is activated to supply deficit power depending on the SOC of the BESS.

As has been discussed, the BESS is operated for immediate power management due to its faster transient response; hence it is established as a major component of the power management control scheme. There are certain limitations of the system which may be addressed in future research although some assumptions were made in this thesis that did not necessitate the need to account for these limitations. For instance, if the capacity of the storage tank is maxed out and the ELZ cannot operate to convert excess power to hydrogen, and the BESS is fully charged, the WTG pitch controller may be activated to regulate the pitch angle and regulate the excess power generated by the WTG or the excess power may be terminated on a dump load. Also, if the BESS and FC are not able to operate in the case of under generation or increased load, load shedding may occur to accommodate for the deficit power in the system.

Chapter 5: Conclusion and future work

Conclusion:

Throughout the coming years, renewable energy generation will continue to be installed on power systems around the globe. As renewables that exhibit power intermittency make up larger percentages of the overall power supply, power quality issues are bound to arise. Energy storage systems have been established to provide an efficient, modular solution to these issues. In fact, hybrid energy systems consisting of renewable energy sources and energy systems will continue to be deployed for grid-connected and stand-alone applications. Therefore, this thesis was successful in proposing an effective active power management methodology in a grid-forming enabled stand-alone system to combat the issue that arises due to the imbalance between energy generation and demand in a hybrid to ensure stable operation of the system. The system modelled was a type-4 wind turbine with hydrogen energy storage (i.e., fuel cell, electrolyzer, storage tank) and battery energy storage. The energy storage systems work to maintain the balance between demand and supply by regulating the DC link voltage according to their storage limits. The system was tested for different cases, considering wind and load variations using PSCAD.

Future Work:

While this thesis has been successful in modeling and demonstrating the operation of the energy storage in active power management of a hybrid energy system consisting of a wind turbine, hydrogen, and battery energy storage, more case studies could be carried out with other energy sources such as solar, etc. included in the hybrid system to model the dynamics of multiple energy sources more accurately. The base model was built with PSCAD and can be remodeled to include other energy sources Also, case studies can be carried out for more

diverse scenarios, such as in the existence of a weak grid, low short circuit ratio or unbalanced load conditions. Furthermore, future work could be done on making the management method more intelligent using artificial intelligence algorithms to accurately dispatch power from accurate predictions which could yield greater efficiency of the system.

References

[1] H. Ritchie and M. Roser, "Access to Energy," Our World in Data.

[2] M. Nicola, Z. Alsafi, C. Sohrabi, A. Kerwan, A. Al-Jabir, C. Losifidis, M. Agha and R. Agha , "The socio-economic implications of the coronavirous pandemic (COVID-19): A review," *Elsevier Public Health Emergency Collectio,* pp. 185-193, 2020 June.

[3] P. Nema, R. Nema and S. Rangnekar, "A current and future state of art development of hybrid energy system using wind and PV-solar: A review," *Renewable and Sustainable Energy Reviews,* vol. 13, no. 8, pp. 2096-2103, 2009.

[4] GWEC, "Global Wind Energy Outlook 2014," October 2014 [Online].

[5] T. Ackerman, Wind in Power Systems, Germany: John Wiley & Sons, 2012.

[6] S. Alam, S. Al-Ismail, A. Salem and M. Abido, "High-Level Penetration of Renewable Energy Sources Into Grid Utility: Challenges and Solutions," *IEEE Access,* pp. 190277-190299, 2020.

[7] C. N. Bhende, S. Mishra and S. G. Malla, "Permanent Magnet Synchronous Generator-Based Standalone Wind Energy Supply System," *IEEE Transactions on Sustainable Energy,* vol. 2, no. 4, pp. 361-373, 2011.

[8] S. Alhejaj and F. Gonzalez-Longatt, "Investigation on Grid-Scale BESS Providing Inertial Response Support".

[9] Y.-W. Shen, D.-P. Ke, Y.-Z. Sun, K. Daniel, W. Qiao and X.-T. Deng, "Advanced Auxiliary Control of an Energy Storage Device for Transient Voltage Support of a Doubly Fed Induction Generator," *IEEE TRANSACTIONS ON SUSTAINABLE ENERGY.*

[10] M. Pellow, C. Emmott, C. Banhart and S. Benson, "Hydrogen or batteries for grid storage? A net energy analysis," *Energy & Environmental Science Journal* , no. 7, 2015.

[11] O. o. E. E. a. R. Energy, "Hydrogen Production: Natural Gas Reforming," Energy.gov, https://www.energy.gov/eere/fuelcells/hydrogen-production-natural-gas-reforming. [Online].

[12] J. Machowski, J. Bailek and J. Bumby, "Frequency stability and wind technologies," *IEEE Trans. Power Syst.,* vol. 20, no. 4, pp. 1905-1903, 2005.

[13] W. Du, F. Tuffner, K. Schneider, R. H. Lasseter, J. Xie, Z. Chen and B. Bhattaria,

"Modelliing of Grid-Forming and Grid-Following Inverters for Dynamic Simulation of Large Scale Distribution Systems," *IEEE Transactions on Power Delivery,* pp. 1-11, 2020.

[14] W. D. Gao, Energy storage for sustainable microgrid, London: Elsevier, 2015.

[15] S. Muyeen, M. Hassan Ali, R. Takahashi, T. Murata, J. Tamura , Y. Tomaka, H. Sakahara and E. Sasano, "Comparative study on transient stability analysis of wind turbine generator system using different drive train models," *IET Renewable Power Generation,* vol. 1, no. 2, pp. 131-141, 2007.

[16] M. Yin, G. Li, M. Zhou and C. Zhao, Modeling of the Wind Turbine with a Permanent Magnet Synchronous Generator for Integration.

[17] M. Haque, K. Muttaqi and M. Negnevitsky, "Control of a Standalone Variable Speed Wind Turbine with a Permanent Magnet Synchronous Generator".

[18] Y. Song, Y. Chen, S. Huang, Z. Yu and Y. Qiao, "Average Value Model of Grid Side Converter in PMSG for System-Level Studies," *The Journal of Engineering,* 2017.

[19] O. Tremblay, L.-A. Dessiant and A.-I. Dekkiche, "A generic battery model for the dynamic simulation of hybrid electric vehicles," Electrical Engineering Department, Ecole de Technologie Superieure.

[20] O. Uleberg, "Modelling of advanced alkaline electrolyzers: a system simulation approach," *International Journal of Hydrogen Energy,* pp. 21-33, 2003.

[21] E. Ezeodili, J. Kim, E. Muljadi and R. Nelms, "Coordinated Power Balance Scheme for a Wind-to-Hydrogen Set in Standalone," in *2020 IEEE Energy Conversion Congress and Exposition (ECCE)*, Detroit, MI, USA, Power Systems.

[22] T. Zhou, B. Francois, M. e. H. Lebbal and S. Lecoeuche, "Real-time emulation of a hydrogen production process for assessment of an active wind energy conversion system," *IEEE Transactions of Industrial Electronics,* vol. 56, no. 3, pp. 737-746, 2009.

[23] P. Artuso, R. Gammon, F. Orecchini and S. Watson, "Alkaline electrolysers: Model and real datqa analysis," *International Journal of Hydrogen Energy,* vol. 36, pp. 7956-7962, 2011.

[24] R. K. Sharma and S. Mishara, "Dynamic power management and control of PV PEM fuel cell based standalone AC/DC microgrid using hybrid energy storage," *IEEE Transactions on Industry Applications.*

[25] R. Lasseter, Z. Chen and D. Pattabiraman, "Grid-Forming Inverters: A Critical Asset for the Power Grid," *IEEE JOURNAL OF EMERGING AND SELECTED TOPICS IN POWER*

ELECTRONICS, vol. 8, no. 2, pp. 925-935, 2020.

[26] T. Zhou and B. Francois, "Energy management and power control of a hybrid active wind generator for distributed power generation and grid integration," *IEEE Transactions on Industrial Electronics,* vol. 58, no. 1, pp. 95-104, 2011.

[27] M. Rezkallah, A. Chandra, B. Singh and R. Niwas, "Modified PQ control for power quality improvement of standalone hybrid wind diesel battery system".

[28] T. Zhao and Z. Ding, "Cooperative optimal control of battery eergy storage system under wind uncertainties in a microgrid," *IEEE Transactions on Power Systems,* vol. 33, no. 2, pp. 2292-2300, 2018.

[29] N. Mohan, Power Electronics: Converters, Applications and Design., Hoboken, NJ: Wiley, 2002.

[30] N. Gyawali and Y. Ohsawa, "Integrating Fuel Cell/Electrolyzer/Ultracapacitor System Into a Stand-Alone Microhydro Plant," *IEEE TRANSACTIONS ON ENERGY CONVERSION,* vol. 25, no. 4, pp. 1092-1011, 2010.

[31] T. Wildi, Electrical machines, drives, and power systems, Essex: Pearson Education Limited, 2014.

[32] "Solar Industry Research Data," Solar Energy Industries Association (SEIA), 2020.

[33] D. Rekioua, Hybrid renewable energy systems: optimization and power managment control, Bejaja, Algeria: Springer.

[34] PSCAD, "Type 2 Wind Turbine Generators," Manitoba Hydro International Ltd, [Online]. Available: https://www.pscad.com/knowledge-base/article/225.

[35] N. A. Luu, "Control and management strategies for a microgrid (PhD Thesis)," 2014.

[36] C. Thomas, M. Akorede, O. Ogunbiyi, B. Olufeagba and J. Samuel, "A Study of Energy Conversion at the Jebba Hydroelectric Power Station," in *IEEE 3rd International Conference on Electro-Technology for National Development (NIGERCON),* 2017.

[37] E. Muljadi and Y.-H. Yu, "Review of Marine Hydrokinetic Power Generation and Power Plant," *Electric Power Components and Systems,* vol. 43, no. 12, pp. 1422-1433, 2015.

[38] F. Rahman, S. Rehman and M. A. Abdul-Majeed, "Overview of energy storage systems for storing electricity from renewable energy sources in Saudi Arabia," *Renewable and*

Sustainable Energy Reviews, vol. 16, pp. 274-283, 2012.

[39] H. R. Esmaeilian and R. Fadaeinedjad, "Resolving power quality issues raised by aerodynaic aspects of wind turbine in isolated microgrids using fuel cell/electrolyzer system.," *IEEE transactions on sustainable energy.*

[40] L. Gandia, G. Arzamendi and P. Dieguez, "Water Electrolysis Technologies in Renewable Hydrogen Technologies," *Science Direct,* pp. 19-41, 2013.

[41] M. Idoia, A. Ursua and P. Sanchis, "Modelling of PEM Fuel Cell Performance: Steady State and Dynamic Experimental Validation," *Energies,* pp. 670-700, 2014.

[42] M. Elamari, "Optimisation of Photovoltaic Powered Electrolysis for Hydrogen Production for a Remote Area in Libya," 2011.

[43] J. Kim, E. Muljadi, V. Gevorgian and A. Hoke, "Dynamic Capabilities of an Energy Storage-Embedded DFIG System," *IEEE Transactions on Industry Applications,* vol. 55, no. 4, pp. 4124-4134, 2019.

[44] M. Khan and M. Iqbal, "Dynamic Modelling, Simulation and Control of a Small Wind-Fuel Cell Hybrid Energy System for Standalone Applications," Faculty of Engineering and Applied Science, Memorial University of Newfoundland, 2004.

[45] C. Wang and H. Nehrir, "A Physically Based Dynamic Model for Solid Oxide Fuel Cells," *IEEE TRANSACTIONS ON ENERGY CONVERSION,* vol. 22, no. 4, pp. 887-898, 2007.

[46] R. Jeevajothi and D. Devaraj, "A new approach for constant DC link voltage in a direct drive variable speed wind energy conversion system," *Journal of Electrical Engineering and Technology,* vol. 10, no. 2, pp. 529-538, 2015.

[47] A. Rahim, S. A. Tijani, M. Fadhulullah, S. Hanapi and K. Sainan, "Optimization of Direct Coupling Solar PV Panel and Advanced Alkaline Electrolyzer System," *Energy Procedia,* vol. 79, pp. 204-211, 2015.

[48] M. El-Sharkh, M. Rahman, A. Alam and M.S, "A dynamic model for a stand-alone PEMfuel cell power plant for residential applications," *Journal of Power Sources,* vol. 138, no. 1-2, pp. 199-204, 2004.

[49] P. Nema, "A current and future state of art development of hybrid energy system using wind and PV-solar: A review," *Renewable and Sustainable Energy Reviews,* vol. 10, 2009.

[50] R. Takahashi, "Output Power Smoothing and Hydrogen Production by using variable speed

wind generators," *IEEE Trans. Industrial Electronics*, 2010.

[51] B. K. Poolla, D. Grob and F. Dorfler, "Placement and implementation of Grid-Forming and Grid-Following virtial inertia and fast frequency response.," *IEEE Transaction on Power Systems*, vol. 34, no. 4, pp. 3035-3046, 2019.

[52] A. Tayyebi, D. Grob, A. Anta, F. Kupzog and F. Dorflier, "Frequency stability of synchronous machines and Grid-Forming power converters," *IEEE Journal of emerging and selected topics in power electronics*, vol. 8, no. 2, pp. 1004-1019, 2020.

[53] D. Pan, X. Wang, F. Liu and R. Shi, "Transient stability of voltage source converters with grid-forming control: a design-oriented study," *IEEE journal of emerging and selected topics in power electronics*, vol. 8, no. 2, pp. 1019-1034, 2020.

Appendix:

A. Table 2: System Parameters:

Wind Turbine Parameters:

Parameter	**Symbol**	**Value**
Rated wind speed	V_{rated}	12m/s
Rated Power	$P_{w\text{-}rated}$	5MW
Radius of wind turbine	$R_{turbine}$	54.84m
Rated Turbine Speed	$w_{t\text{-}rated}$	2.177 rad/s
Turbine Torque	T_a	0.833pu
Maximum Power Coefficient	C_{pmax}	0.50
Drive Characteristics		
Parameter	**Symbol**	**Value**
Damping constant,	D_t	1
Shaft stiffness,	K	0.5
Turbine inertia,	H_t	3.5s
PMSG		
Parameter	**Symbol**	**Value**
Rated PMSG Power	$P_{g\text{-}rated}$	5MW
Rated voltage	V_{rated}	0.69KV
d axis reactance,	X_d	0.55 p.u.
q axis reactance,	X_q	1.11 p.u.
rated frequency	f_{rated}	30 Hz

Battery Energy Storage Parameters:

Parameter	**Value**
Nominal voltage	1.45KV
Rated Capacity	0.065KAh
Nominal capacity	0.95 p.u.
Voltage at exponential point	1.03 p.u.
Fully charged voltage	1.15 p.u
Rated Capacity	0.065KAh

Electrolyzer System Parameters:

Parameters	**Symbols**	**Value**
Reversible Voltage	V_{rev}	1.229 V
Area of Electrodes	A	0.25 m^2
Faraday's Constant	F	96485 C/mol
Number of Electrons	Z	2
Coefficient for Overvoltage on Electrodes	s	0.185 V
	τ_1	1.002 A^{-1} m^2
	τ_2	8.424 A^{-1} m^2 ℃
	τ_3	247.3 A^{-1} m^2 $℃^2$
Ohmic resistance of electrolyte parameters	r_1	8.05e-5 Ω m^2
	r_2	-2.5e-7 Ω m^2 ℃

Compressor and Tank model parameters:

Symbol	Value
Cm	2
αeff	0.7
k	2
T_{tank}	25°C
V_{tank}	5L

PEM FC parameters:

Symbol	Value
R^{int}	0.00303Ω
B_1	$0.04777A^{-1}$
B_2	0.0136 V
k_r	$0.966x10^{-6}$
r_{HO}	1.168
k_{H_2}	$4.22x10^{-5}kmols^{-1}atm$
k_{O_2}	$2.11x10^{-5}kmols^{-1}atm$
k_{H_2O}	$7.72x10^{-6}kmols^{-1}atm$
τ_{H_2}	3.37s
τ_{O_2}	6.74s
τ_{H_2O}	18.418s

B. Park transformation

The dq0 transformation, also called park transformation is a vector space transformation of three-phase time domain signals from stationary phase coordinate system (ABC) to a rotating coordinate system (dq0). This transformation helps remove the time-variant coefficients. The transformation matrix and the inverse transformation matrix are defined as follows [31]:

$$A = \begin{bmatrix} \cos(\theta) & -\sin(\theta) & 1 \\ \cos(\theta - \frac{2\pi}{3}) & -\sin(\theta - \frac{2\pi}{3}) & 1 \\ \cos(\theta + \frac{2\pi}{3}) & -\sin(\theta + \frac{2\pi}{3}) & 1 \end{bmatrix} \tag{67}$$

$$A^{-1} = \frac{2}{3}\begin{bmatrix} \cos(\theta) & \cos(\theta - \frac{2\pi}{3}) & \cos(\theta + \frac{2\pi}{3}) \\ -\sin(\theta) & -\sin(\theta - \frac{2\pi}{3}) & -\sin(\theta + \frac{2\pi}{3}) \\ \frac{1}{2} & \frac{1}{2} & \frac{1}{2} \end{bmatrix} \tag{68}$$

where θ is the angle between the rotating and fixed coordinate system. The graphical representation of the corresponding vectors is depicted below:

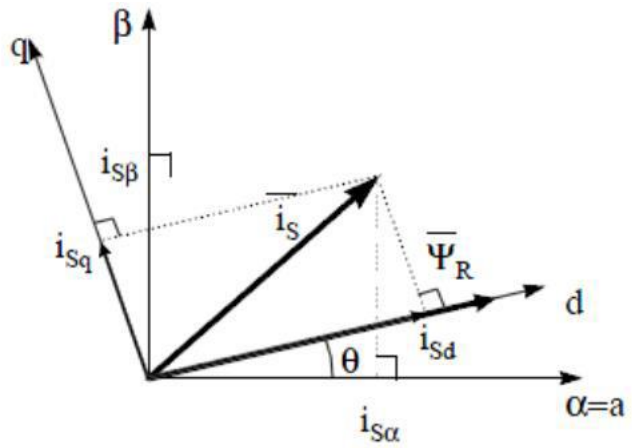

Figure 30: Representation of park transformation

The relation between the variables in the abc frame and the new variables in the dq0 frame are thus:

$$V_{dq0} = A.V_{abc} \tag{69}$$

$$V_{abc} = A^{-1}.V_{dq0} \tag{70}$$

where:

$$V_{abc} = \begin{bmatrix} V_a \\ V_b \\ V_c \end{bmatrix}, V_{dq0} = \begin{bmatrix} V_d \\ V_q \\ V_0 \end{bmatrix}$$